Molecular Therapy
Original Article

Modification of the VP1u region boosts transduction of adeno-associated virus vectors for ocular gene therapy

Mengtian Cui,[1,2] Shun-Yun Cheng,[1,3] Jialing Liang,[1,2] Jackson McGowan,[1] Meiyu Xu,[1] Guangchao Xu,[1,4,5,6] Li Luo,[1,4,7,8] Joae Wu,[9] Christine D. Harman,[10] Amanda L. Jacobson,[10] Lydia E. Kapeller,[10] Melaney A. Mayes,[10] Suk Namkung,[1,2] Tapan Sharma,[1,2] Thomas B. Leland,[1,2] Fang Zhang,[1,2] Mitchell Yip,[1] Brian Rossmiller,[1] Thomas Xue,[1] Xiupeng Chen,[1,2] Wassamon Boonying,[1,2] Anoushka Lotun,[1,2] Dan Wang,[1,2,11] Qin Su,[1] Jun Xie,[1,2,12] Yuquan Wei,[4] Ann M. Rothstein,[13] Meredith S. Gregory-Ksander,[14] Andras Komaromy,[10] Bo Tian,[1,3] Haijiang Lin,[1,3] Claudio Punzo,[1,3] Phillip W.L. Tai,[1,2,12] and Guangping Gao[1,2,12]

[1]Horae Gene Therapy Center, UMass Chan Medical School, Worcester, MA 01605, USA; [2]Department of Genetic and Cellular Medicine, UMass Chan Medical School, Worcester, MA 01605, USA; [3]Department of Ophthalmology and Visual Sciences, UMass Chan Medical School, Worcester, MA 01605, USA; [4]State Key Laboratory of Biotherapy, West China Hospital, Sichuan University, Chengdu 610041, P.R. China; [5]Department of Burns and Plastic Surgery, Affiliated Hospital of Zunyi Medical University, Zunyi 563003, P.R. China; [6]The Collaborative Innovation Center of Tissue Damage Repair and Regeneration Medicine, Zunyi Medical University, Zunyi 563003, P.R. China; [7]Center for Reproductive Medicine, Department of Gynecology and Obstetrics, West China Second University Hospital, Sichuan University, Chengdu 610041, P.R. China; [8]Key Laboratory of Birth Defects and Related Diseases of Women and Children (Sichuan University), Ministry of Education, Chengdu 610041, P.R. China; [9]Biochemistry and Molecular Biotechnology, UMass Chan Medical School, Worcester, MA, USA; [10]Department of Small Animal Clinical Sciences, College of Veterinary Medicine, Michigan State University, East Lansing, MI 48824, USA; [11]RNA Therapeutics Institute, UMass Chan Medical School, Worcester, MA 01605, USA; [12]Department of Microbiology, UMass Chan Medical School, Worcester, MA 01605, USA; [13]Department of Medicine, UMass Chan Medical School, Worcester, MA 01605, USA; [14]Schepens Eye Research Institute of Mass Eye and Ear, Department of Ophthalmology, Harvard Medical School, Worcester, MA 01605, USA

Adeno-associated virus (AAV) capsids that can confer efficient and safe gene therapy of the retina remain unmet needs. In this study, we isolated a library of natural capsids from human tissues and identified two variants that conferred strong transduction of retinal tissues following intravitreal injections into mice and non-human primates. Interestingly, the defining amino acids among the two variants are located within the luminal VP1 unique (VP1u) region of the capsid. Combining these defining residues into a single capsid (AAV2.MC1) had an additive effect. We demonstrated that the MC1 modification enhances intracellular trafficking and nuclear entry. Importantly, we provide proof of concept that the AAV2.MC1 capsid can deliver an anti-vascular endothelial growth factor (VEGF) transgene to treat wet age-related macular degeneration. Finally, we demonstrate that the modification can also be grafted onto other AAV serotypes to boost baseline transduction. These findings open up new avenues for capsid modification through targeted alterations of the VP1u region.

INTRODUCTION

Adeno-associated viruses (AAVs) are small, non-enveloped, single-stranded DNA (ssDNA) viruses belonging to the *Parvoviridae* family.[1] The wild-type AAV genome encodes four known open reading frames (ORFs): *rep*, *cap*, the assembly activating protein (*AAP*), and the membrane-associated accessory protein (*MAAP*).[2–4] The *cap* ORF encodes for three capsid subunits (VP1, VP2, and VP3), which assemble into a 60-mer icosahedral capsid at an approximate ratio of 1:1:10.[2,4] The structural topology of the AAV capsid is predominantly defined by the VP3 domain; thus, VP3 is widely believed to govern tissue tropism by directly interacting with cell surface receptors.[5,6]

In the past decade, recombinant AAVs (rAAVs) have become the most popular gene therapy vehicle, having notable success for treating ophthalmological diseases.[7–10] However, the current suite of capsids that can efficiently and safely transduce the retina is limited. Furthermore, cell-type-tropic capsids for gene therapy remain an unmet need. For example, ganglion cells are targets for treating glaucoma and Leber hereditary optic neuropathy (LHON),[11,12] bipolar cells are targets for treating retinitis pigmentosa,[13] and photoreceptors and retinal pigment epithelium (RPE) cells are targets for Stargardt disease,[14]

Received 13 October 2025; accepted 22 January 2026;
https://doi.org/10.1016/j.ymthe.2026.01.029.

Correspondence: Phillip W.L. Tai, Horae Gene Therapy Center, UMass Chan Medical School, Worcester, MA 01605, USA.
E-mail: phillip.tai2@umassmed.edu
Correspondence: Guangping Gao, Horae Gene Therapy Center, UMass Chan Medical School, Worcester, MA 01605, USA.
E-mail: guangping.gao@umassmed.edu

RPE65-associated inherited retinal dystrophy,[15] and others. Serotype 2 (AAV2) remains the most utilized in preclinical studies.[16] Subretinal injection of an AAV2 vector to target RPE cells is the basis of Luxterna (voretigene neparvovec) the gene therapy for Leber's congenital amaurosis.[17] An engineered capsid that carries a peptide insert at the most surface-exposed domain of the AAV capsid (loop VIII), called AAV2.7m8, was developed to transduce photoreceptor cells following intravitreal (i.v.t.) delivery.[18] However, AAV2.7m8 is reported to also trigger inflammation in certain contexts.[19–22]

Over the past decade, various approaches have emerged for developing novel AAV capsids.[1,23] Natural serotypes identified from humans and non-human primates (NHPs) have yielded a large selection of capsids that have been tested for research and used in the clinic.[16] Although more advanced methods for synthesizing and screening engineered capsids have been proven to produce highly potent capsids,[16] naturally derived capsids can still reveal unique tropism profiles and novel aspects of AAV biology. For instance, our previous work identified an AAV2 variant with tropism to the CNS, called AAV2.v66.[24]

One distinct advantage of natural capsids is that novel features are not restricted to surface-exposed residues, as is the case with most directed evolution and rational design strategies.[25] The largest *cap* transcript encodes VP1, a protein that contains a 137- to 138-amino acid domain that is unique from VP2 and VP3, called VP1 unique (VP1u). The VP1u region is highly conserved among the known serotypes and within the broader parvovirus family.[26,27] It is hypothesized to be crucial for multiple post-entry steps during AAV infection.[28,29] VP1u is positioned inside the lumen of a newly assembled AAV virion. Following endocytosis and retrograde trafficking, the pH environment for AAVs decreases from 7.0 to around 4.5 in late endosomes (LEs) and lysosomes. During acidification, VP1u is extruded out of the AAV capsid, exposing its phospholipase A_2 (PLA_2) domain. The PLA_2 domain is hypothesized to drive escape into the cytosol.[30] The VP1u region also carries a domain that associates with GPR108, the conserved entry factor localized to the *trans*-Golgi network (TGN).[31] It has been hypothesized that GPR108 plays a role in vector escape by stabilizing the extruded VP1u, promoting the release of vectors from the TGN rather than from the endosomal compartment.[31,32] The VP1u and VP1/VP2 common regions also contain three basic regions (BR1–BR3), which serve as nuclear localization sequences (NLSs). Recently, the VP1u region of AAV8 was reported to be involved in transcription of packaged transgenes.[33] Nevertheless, the VP1u domain remains largely unexplored as a target region for capsid engineering and continues to be understudied.

In this report, we screened a library of human-derived AAV2 variants and identified two capsids that were able to transduce mouse and NHP retinas better than other AAV2 variants. Interestingly, the two variants only carry residues that differ from prototypical AAV2 in the VP1u region. We combined the defining residues into a single capsid, named AAV2.MC1, and showed that it can strongly transduce mouse, canine, and NHP retinas following i.v.t. injection. We also found that the MC1 modification can improve intracellular trafficking kinetics of AAV2. Given these improvements, we demonstrated that AAV2.MC1 can be used to deliver an anti-vascular endothelial growth factor (VEGF) transgene to treat wet age-related macular degeneration (AMD) using a laser-induced choroidal neovascularization mouse model. Since VP1u is highly conserved among AAVs, we showed that the MC1 modification can also be applied to other serotypes and engineered capsids to boost baseline transduction in a context-dependent manner. These mechanistic insights contribute to a deeper understanding of VP1u and provide valuable guidance for capsid engineering strategies.

RESULTS

Novel human tissue-derived AAV capsid identification and generation of an AAV2 variant library

We previously obtained 728 tumor and adjacent non-lesion resection samples from 413 cancer patients receiving care at West China Hospital (Chengdu, China).[34] Using two rounds of high-cycle PCR with primers flanking the AAV2 *rep-cap* or *cap* ORFs, followed by single-molecule, real-time (SMRT) sequencing, we identified 425 unique proviral capsid sequences with similarities to prototypical AAV2. These variants were individually cloned into packaging plasmids containing *rep* from AAV2.[1] The plasmids were then used in small-scale triple-plasmid transfections of HEK293 cells to test their ability to package transgene vectors. We found that 26% of the capsids had packaging yields that were equivalent to or better than AAV2. 59% of the capsids showed a tenth of AAV2's packaging yield or more (Figure 1A). Since production costs and manufacturing limitations are current barriers for many gene therapy programs, we selected 86 capsids with packaging yields greater than AAV2 and individually packaged them with an enhanced green fluorescent protein reporter transgene containing unique barcodes inserted into the 3′ UTR (*CB6-Egfp-bc*) (File S1). When coupled with next-generation sequencing (NGS), the barcodes permitted the differential detection of vector genomes and transcripts within samples. During purification steps, the vectors were pooled together and purified as a single vector batch.

Identification of AAV2 variants with strong transduction of mouse and NHP retinas following i.v.t. injection

We aimed to screen the AAV2 variant library for capsids that can strongly transduce the mouse retina following subretinal (s.r.) and i.v.t. injections. The AAV2 variant library was spiked with AAV2 packaged with a similarly 3′ UTR-barcoded *Egfp* transgene cassette. One month post injection, NGS detection and tabulation of barcodes were performed on transduced retinas as a direct readout of vector genome abundances (DNA library) or transgene transcript abundances (RNA/cDNA library) in tissues (File S1). Overall, we found that multiple variants were able to transduce the retina better than AAV2 following s.r. injection (Figure 1B). However, we found only four capsids that stood out over other variants when delivered by i.v.t.: variant 149 (AAV2.v149), variant 152 (AAV2.v152), variant 175 (AAV2.v175), and variant 182 (AAV2.v182). Notably,

Please cite this article in press as: Cui et al., Modification of the VP1u region boosts transduction of adeno-associated virus vectors for ocular gene therapy, Molecular Therapy (2026), https://doi.org/10.1016/j.ymthe.2026.01.029

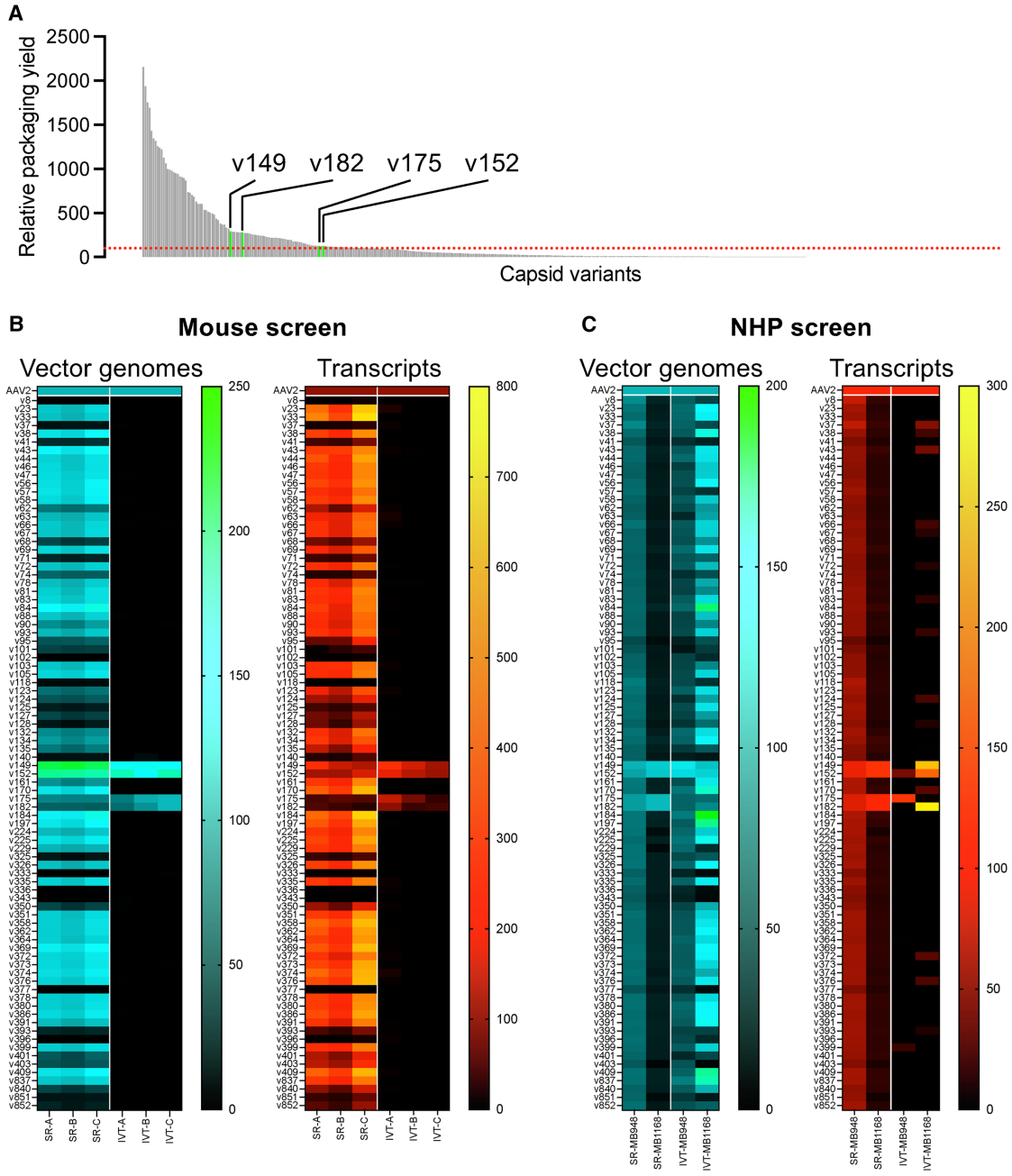

Figure 1. Identification of four AAV2 variants that strongly transduce retinas

(A) Waterfall plot displaying packaging yields of AAV2 variants. qPCR analyses were performed on crude lysates obtained from HEK293 cells subjected to standard triple-plasmid transfection for generating AAV vectors. Four variants (AAV2.v149, AAV2.v152, AAV2.v175, and AAV2.v182) identified by *in vivo* screening are highlighted. Red line, 100. (B and C) Heatmaps of vector barcode abundance in retinal tissues of library-transduced mouse retinas (n = 3, B) and NHP retinas (n = 2, C). The detection of vector genomes (left heatmaps) and transcript (right heatmaps) are depicted for each of the 86 candidate vectors. Vectors were tested by subretinal (s.r.) and intravitreal (i.v.t.) injections. The transduction profile of prototypical AAV2 is set to 100. Value scales are depicted to the right of each heatmap. NHP IDs (MB948 and MB1168) are annotated for each column.

AAV2.v149 and AAV2.v152 showed 2-fold more vector genomes than AAV2 by s.r. delivery (Figure S1A). The transgene transcript levels from these variants were also higher.

We also screened the AAV2 variant library in NHPs. In this study, two animals were administered the capsid library, where one eye was treated by s.r. and the other eye by i.v.t. (5.0E11 vg/eye). Similar

Please cite this article in press as: Cui et al., Modification of the VP1u region boosts transduction of adeno-associated virus vectors for ocular gene therapy, Molecular Therapy (2026), https://doi.org/10.1016/j.ymthe.2026.01.029

to the outcomes in mice, only AAV2.v149, AAV2.v152, AAV2.v175, and AAV2.v182 seemed to strongly transduce NHP retinas (Figure 1C). In contrast to the results observed in mice, s.r. injections in NHPs did not reveal any capsids with stronger transduction profiles than conferred by AAV2. It should be noted that transductions were variable between animals. For instance, AAV2.v149 and AAV2.v182 exhibited approximately 2.5-fold and 3-fold stronger transduction than AAV2 in the i.v.t.-injected eye of one animal (MB1168) but near background levels in the other (MB948) (Figures 1C and S1B).

Measuring transduction profiles of the AAV2 variants

We sought to test the four AAV2 variants for their ability to transduce cells *in vitro*. Vectors were packaged with a standard self-complementary (sc)*CB6-Egfp* transgene cassette.[35] We first tested non-purified vectors obtained from triple-plasmid-transfected HEK293 cells (crude lysates). Transductions of HeLa cells by crude lysates with AAV2.v149 and AAV2.v152 vectors were greater than what was achieved by crude lysates with AAV2 vectors (Figure 2A). In contrast, those with AAV2.v175 and AAV2.v182 vectors appeared slightly weaker. Given that the variants from crude lysates were able to transduce cells *in vitro*, we purified the vectors by cesium chloride (CsCl) density gradient ultracentrifugation and transduced them into HeLa cells. Cell transductions were then assayed by flow cytometry. While AAV2 transduced 20% of cells by 24 h (Figure 2B), AAV2.v149 and AAV2.v152 vectors transduced nearly 50% of cells. On the other hand, both AAV2.v175 and AAV2.v182 vectors transduced about 25% of cells (Figure 2B). Mean fluorescence intensities showed that AAV2.v149 and AAV2.v152 vectors yielded ∼40% more signal (Figure 2C), while AAV2.v175 and AAV2.v182 vectors showed a marginal decrease in signal. We next tested the variants by i.v.t. injection in adult mice. After 1 month, we observed substantially better transduction by AAV2.v149 and AAV2.v152 vectors than by AAV2, while AAV2.v175 and AAV2.v182 vectors showed much weaker levels of transduction (Figure 2D).

Combining the defining VP1u residues into a single capsid conferred additive transduction in mouse retinas

Upon characterizing the defining amino acids among the two variants that showed better transduction profiles than AAV2, we discovered that the only amino acids that differed between AAV2 and the two variants were within VP1u (Figure S2). AAV2.v149 harbors two amino acid residues that differ from AAV2 (E36G and V125A), while AAV2.v152 has a single amino acid difference (D80N). Interestingly, the D80N residue is located within the PLA_2 domain, while the V125A residue is located near BR1. The E36G residue is located at the N terminus of the VP1u region, in a region with no established function. Of note, there were 25 residues within the VP1u region alone that were found to be different from AAV2 among the 86 variants (Figure S2).

We next evaluated the contributions of each unique VP1u residue found in AAV2.v149 and AAV2.v152. Using AAV2 as the "scaffold" capsid, we produced three vectors (AAV2.E36G, AAV2.D80N, and AAV2.V125A) packaged with the sc*CB6-Egfp* transgene cassette. The vectors were each injected into mouse eyes by i.v.t. delivery. We also injected eyes with scAAV2.7m8-*CB6-Egfp* for comparison. One month post-injection, we found that all four of the engineered capsids outperformed AAV2 (Figure 3A). Interestingly, the vectors did not show any significant differences in relative vector copies when assayed by Droplet Digital PCR (ddPCR) (Figure 3B). In contrast, detection of *Egfp* transcripts showed that AAV2.E36G, AAV2.D80N, and AAV2.V125A vectors transduced retinas more than 2-fold greater than AAV2 vectors (Figure 3C), while AAV2.7m8 vectors did not show a significant increase.

Knowing that each of the mutated residues increased the transduction of AAV2, we aimed to determine whether combining the E36G, D80N, and V125A mutations into a single capsid would lead to an additive effect. We cloned each mutation into the VP1u region of AAV2 and named the resulting capsid AAV2.MC1. The AAV2.MC1 capsid was then packaged with the sc*CB6-Egfp* transgene to test its ability to transduce the retina. The AAV2.MC1 vector showed a slight but significant increase in vector genomes. Importantly, the AAV2.MC1 vector conferred 6-fold greater detection of *Egfp* transcripts than achieved by the AAV2 vector (Figure 3C). These results suggest that combining the E36G, D80N, and V125A mutations results in an additive effect for transducing mouse retinas.

Since the improvements in transduction primarily resulted in increased transcript levels but not vector genome abundance, we predicted that the MC1 modification may alter intracellular trafficking and nuclear entry but not necessarily cell entry. By calculating transcripts per vector genome, we found that vectors packaged with AAV2.E36G, AAV2.D80N, AAV2.V125A, and AAV2.MC1 showed improvements over AAV2 vectors, while those packaged with AAV2.7m8, which only has alterations of VP3, did not show significant differences from AAV2 vectors (Figure 3D). These results indeed confirm the notion that the variant residues altered intracellular trafficking and not necessarily cell entry.

Retinas that were treated with the AAV2, AAV2.7m8, and AAV2.MC1 vectors were next subjected to cryosectioning and immunohistology to compare differences in the transduction of different retinal layers (Figures 3E–3K). All of the vectors conferred strong transduction of the ganglion cell layer (GCL) and some transduction of the inner nuclear layer (INL). Compared to retinas treated with AAV2, those treated with AAV2.7m8 showed a higher degree of outer plexiform layer (OPL) transduction, where photoreceptor synapses reside. In contrast, vectors packaged with AAV2.MC1 conferred strong transduction throughout several layers of the retina (Figures 3E and 3F). We observed significantly greater percentages of transduced ganglion cells, bipolar cells, horizontal cells, and amacrine cells by AAV.MC1 vectors than achieved by AAV2 vectors (Figures 3G–3J). In contrast, the only cell type among these where AAV2.7m8 vectors showed a higher percentage of transduction than AAV2 vectors was ganglion cells (Figure 3G). Quantification of transduced photoreceptor outer

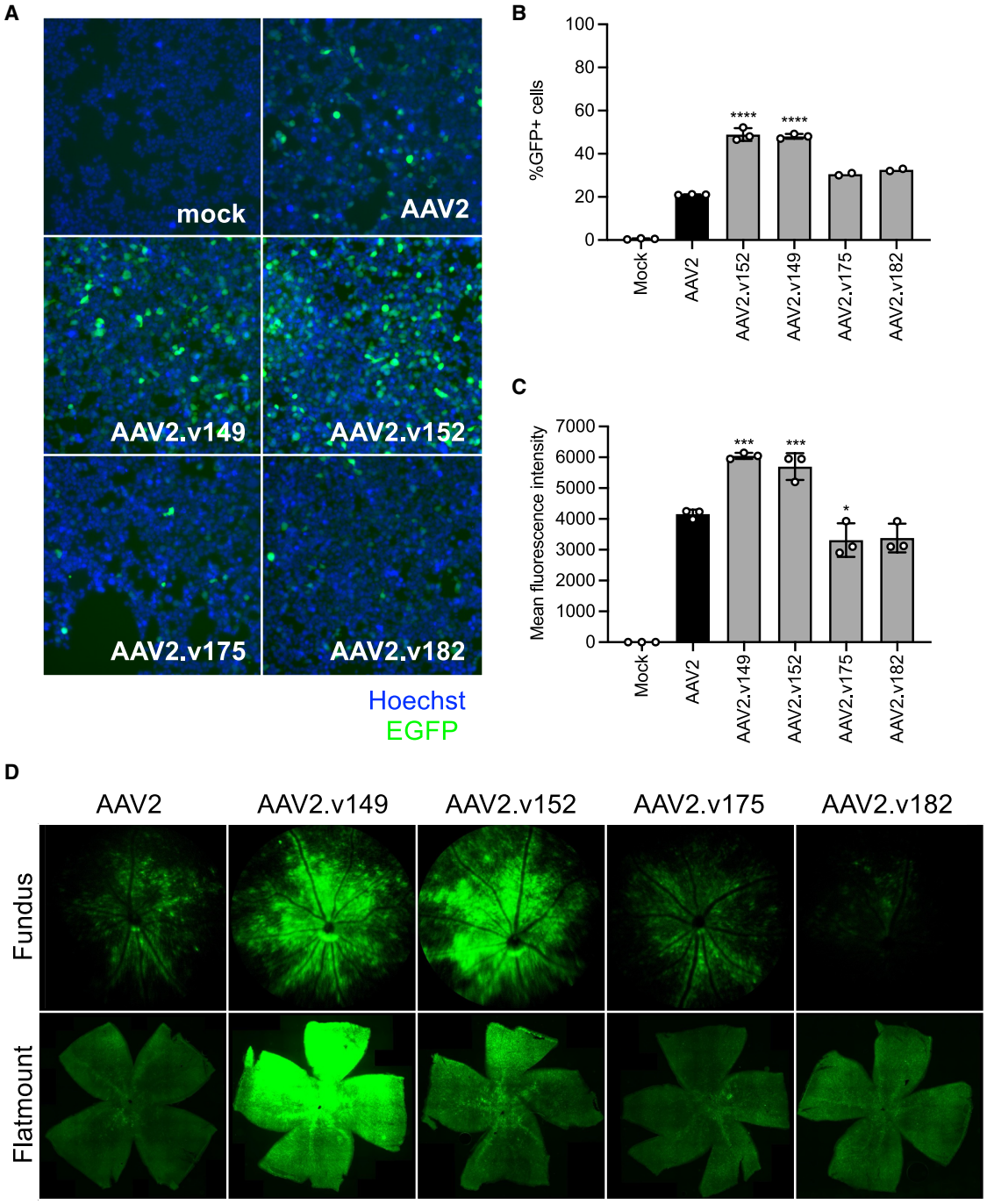

Figure 2. Transduction efficiency of AAV2 variants

(A) Epifluorescence images of HeLa cells treated with scAAV-*Egfp* vectors (from crude lysates of HEK293 cells producing AAV2, AAV2.v149, AAV2.v152, AAV2.v175, or AAV2.v182) with Ad virus (MOI = 100) after 24 h. EGFP (green) and Hoechst dye (blue) mark transduced cells and nuclei, respectively. Non-transduced cell lysate (mock) was used as a negative control. (B and C) Flow cytometry quantification of HeLa cells treated with CsCl-purified scAAV-*Egfp* vectors packaged with the AAV2 variants at an MOI of 5E3 vg/cell. Quantifications by percentage of EGFP-positive cells (B) and mean fluorescence values (C) were assessed 24 h post-transduction. Values represent mean ± SD. $^{*}p < 0.05$, $^{***}p < 0.001$, $^{****}p < 0.0001$. For $n = 2$ samples, statistics were not determined. (D) Representative fundus images (top row) and retinal flat mounts (bottom row) from eyes injected with either the AAV2 vector or vectors packaged with the four AAV2-variants (2.5E8 vg/eye, 1 μL) via i.v.t. administration.

Please cite this article in press as: Cui et al., Modification of the VP1u region boosts transduction of adeno-associated virus vectors for ocular gene therapy, Molecular Therapy (2026), https://doi.org/10.1016/j.ymthe.2026.01.029

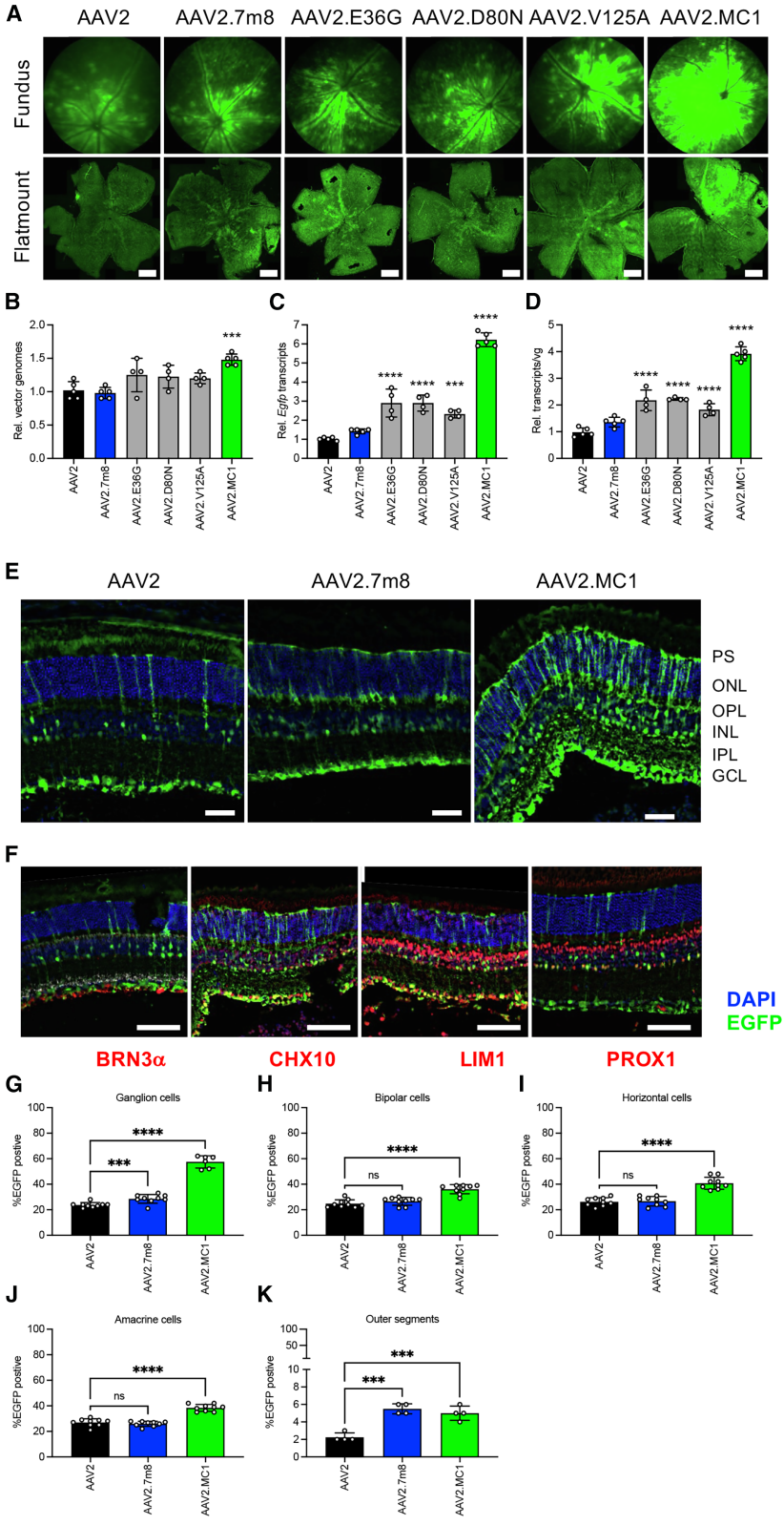

Figure 3. The defining VP1u residues from the AAV2 variants confer increased *in vivo* transduction

(A–D) Mouse retinas were transduced with sc*CB6.PI.EGFP* vectors packaged with AAV2, AAV2.7m8, and AAV2 with single amino acid mutations of individual defining VP1u residues from the two variants (E36G, D80N, and V125A) by i.v.t. injection. (A) One month post-treatment with vectors injected at 1E9 vg/eye, fundus (top row) and flat-mount (bottom row) images were acquired. Scale bar: 1 mm. Retinas were harvested and subjected to ddPCR to quantify relative vector genomes (B) and *Egfp* transcripts (C) in transduced tissues. Relative transcripts per vector genomes (D) were also calculated. (E) Cryosections of treated retinas at 1E9 vg/eye. Sections were stained with an antibody against EGFP (green) and DAPI (DNA, blue). Layers of the eye are marked: photoreceptor segment layer (PS), outer nuclear layer (ONL), outer plexiform layer (OPL), inner nuclear layer (INL), inner plexiform layer (IPL), and ganglion cell layer (GCL). Scale bar: 50 μm. (F and G) Cell type transduction was assessed using antibodies against ganglion cells (BRN3α), bipolar cells (CHX10), horizontal cells (LIM1), and amacrine cells (PROX1). (F) Representative section of an AAV2.MC1 vector-treated retina. Scale bar: 100 μm. (G–J) Quantification of the percentage of EGFP-positive ganglion cells (G), bipolar cells (H), horizontal cells (I), and amacrine cells (J) is displayed as histograms. Transduced outer segments were also counted as a readout of photoreceptor transduction (K). Values represent mean ± SD ($n \geq 4$). ***$p < 0.001$, ****$p < 0.0001$.

Please cite this article in press as: Cui et al., Modification of the VP1u region boosts transduction of adeno-associated virus vectors for ocular gene therapy, Molecular Therapy (2026), https://doi.org/10.1016/j.ymthe.2026.01.029

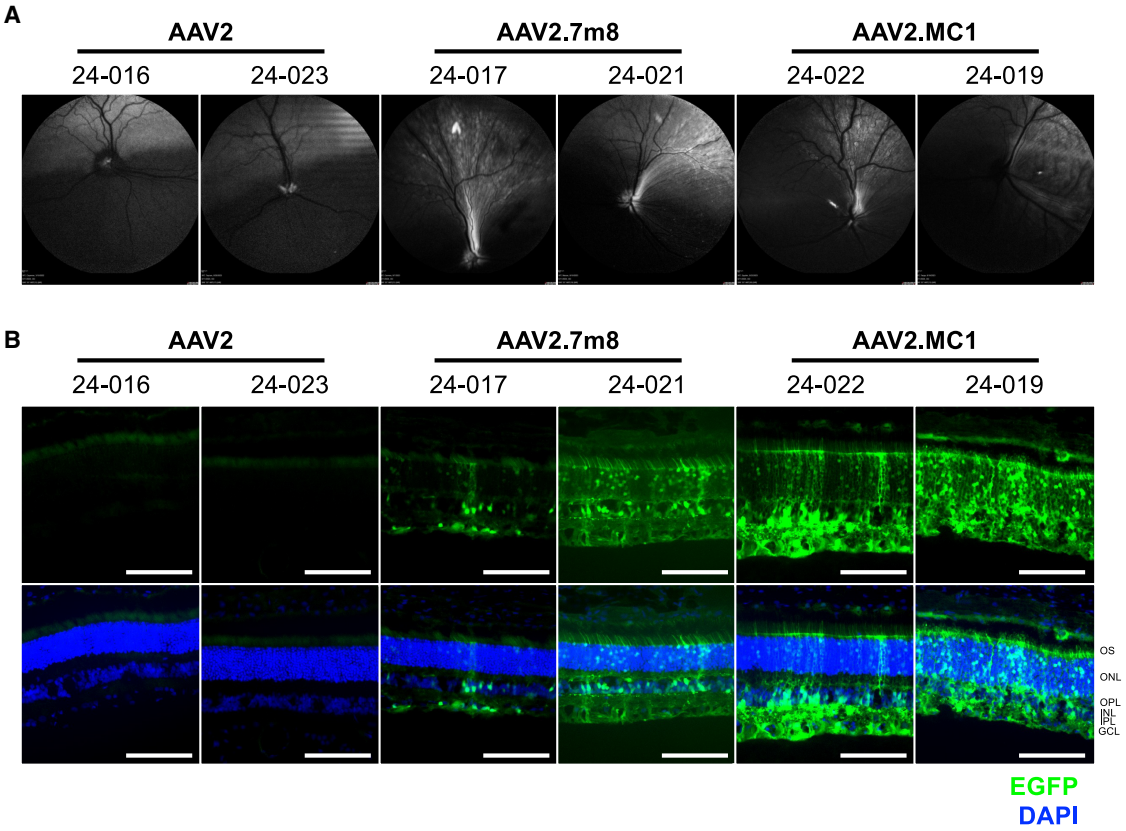

Figure 4. Comparisons of vector transduction in canine retinas by AAV vectors

scCB6-Egfp vectors packaged with AAV2, AAV2.7m8, or AAV2.MC1 were injected into the eyes of two dogs by i.v.t. delivery (1E10 vg/eye). (A) Fundus autofluorescence imaging 1 month post treatment. (B) Cryosections of treated retinas. Sections were stained with antibodies against EGFP (green) and DAPI (DNA, blue). Layers of the retina are marked. Animal IDs are labeled above each panel. Scale bar: 0.1 mm.

segments showed that both AAV.7m8 and AAV.MC1 vectors transduced 2-fold more photoreceptors than vectors packaged with AAV2 (~5% versus 2%) (Figure 3K).

The MC1 modification increases AAV2 vector transduction of retinas in large-animal models

We next aimed to evaluate the ability of AAV2.MC1 to transduce retinal tissues following i.v.t. delivery in large animals. AAV2, AAV2.7m8, and AAV2.MC1 capsids packaged with *scCB6-PI-Egfp* were first administered to wild-type beagle retinas. Each vector was tested in two dogs (one eye each). Four-weeks post-injection, fundus autofluorescence imaging of treated eyes showed that EGFP expression in AAV2-treated eyes was restricted to the optic nerve head (Figure 4A). In contrast, both animals treated with AAV2.7m8 and one of two animals treated with AAV2.MC1 showed EGFP expression that was more widely distributed throughout the retina. However, AAV2.7m8 did confer a broader distribution of transduction across the retina than achieved by AAV2.MC1 (Figure 4A). We also note that there was some intra-group variability, which can be attributed to biological and/or experimental variability. Nevertheless, both AAV2.7m8 and AAV2.MC1 achieved better retinal transduction than prototypical AAV2 when delivered by i.v.t. into canine eyes.

Treated retinas were subsequently harvested, cryosectioned, and stained for EGFP expression to observe transduction penetrance by immunofluorescence microscopy. Again, retinas treated with AAV2 vectors resulted in very poor transduction (Figure 4B). In contrast, both AAV2.7m8 and AAV2.MC1 vectors were able to strongly transduce multiple layers of the retina. The AAV2.MC1 vector appeared to achieve a stronger EGFP signal in the GCL, the INL, and the outer nuclear layer (ONL). Transduction of outer segments was notable, suggesting that the vectors were able to penetrate to the outer layers of the retina. Again, only two eyes were tested for each vector in these experiments, with indications of some biological/experimental variability. Nevertheless, eyes receiving AAV2.MC1 vectors showed stronger transduction of the GCL than those receiving AAV2 or AAV2.7m8 (Figure 4B).

We also sought to examine the transduction profile of the AAV2.MC1 vector in NHP (cynomolgus macaque) eyes following i.v.t. delivery. Unfortunately, due to limited resources, we only tested one animal

Please cite this article in press as: Cui et al., Modification of the VP1u region boosts transduction of adeno-associated virus vectors for ocular gene therapy, Molecular Therapy (2026), https://doi.org/10.1016/j.ymthe.2026.01.029

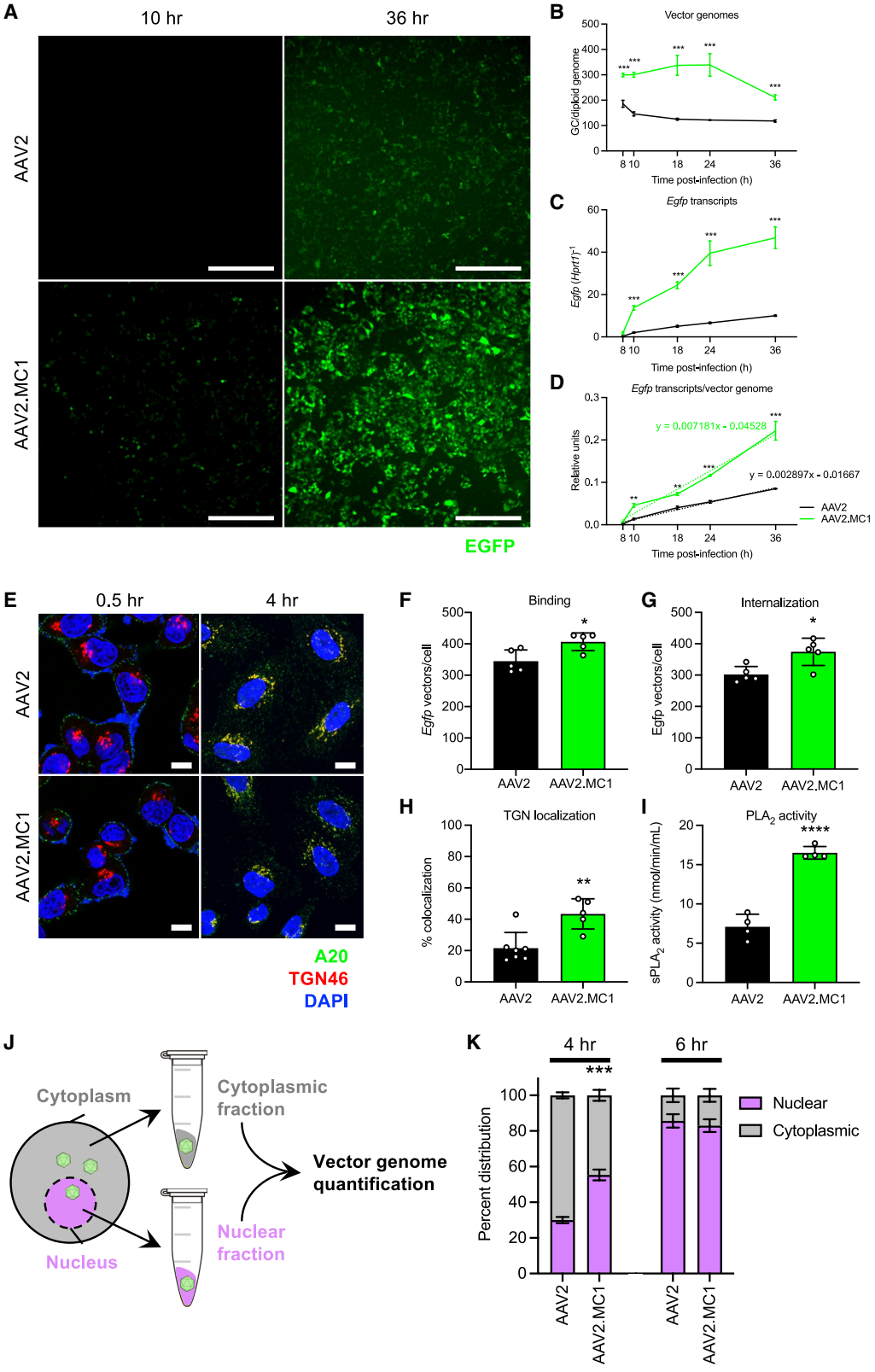

(legend on next page)

by injecting one eye with AAV2 vectors and the other eye with AAV2.MC1 vectors. One month following treatment, fundus autofluorescence imaging did not reveal strong transduction by either vector (Figure S3A). However, we found, by immunofluorescence imaging of cryosections, that AAV2.MC1 conferred a greater area of transduced tissues in the OPL, INL, and IPL than what was achieved by AAV2 (Figures S3B and S3C). One interesting observation was that the percentage of transduced cells in the GCL was similar between the vector-treated eyes (Figure S3C). Nevertheless, transduction by the AAV.MC1 vector resulted in stronger EGFP expression in the GCL than transduction by the AAV2 vector (Figure S3B).

The MC1 modification boosts AAV2 transduction at post-entry steps

We next sought to understand the mechanisms that permitted increased transduction by the MC1 modification. Since the residues that define AAV2.MC1 are all within VP1u, we predicted that the increases in transduction are due to improvements of post-entry mechanisms. Since HeLa cells are a proven cell line to study AAV intracellular trafficking and can be efficiently transduced by AAV2 vectors, AAV post-entry properties were evaluated with HeLa cells.[36] We first compared the transduction of AAV2 and AAV2.MC1 vectors throughout a 36-h time course. HeLa cells were synchronized by pre-chilling at 4°C, transduced with AAV vectors, and moved to 37°C. Cells were collected 8, 10, 18, 24, and 36 h post transduction. 10 h post-transduction, cells transduced with AAV2.MC1 vectors were visibly expressing EGFP, while those transduced with AAV2 vectors were not (Figure 5A). At 36 h, >80% of transduced cells were expressing EGFP in both treatment groups. However, cells treated with the AAV2.MC1 vector showed stronger fluorescence (Figure 5A). AAV2.MC1 vector-transduced cells showed approximately 2-fold more vector genomes than those transduced by the AAV2 vector throughout all collection time points (Figure 5B). Interestingly, cells treated with the AAV2 vector showed a slight decline in detected genomes from 8 to 18 h post-transduction. Cells treated with AAV2.MC1 vectors did not display a decrease in detectable genomes until 24 and 36 h post-treatment. At 10 h, AAV2.MC1 vector-treated cells showed a 6-fold greater abundance of *egfp* transcripts than AAV2 vector-treated cells (Figure 5C). This difference was sustained throughout the course of the study (36 h) despite the vector genomes only exhibiting 2-fold differences (Figure 5B). Calculating each transduction time point by the detection of transcripts per vector genomes present indicated a ∼2.5-fold difference in slopes ($p = 0.001$) (Figure 5D).

We next aimed to determine differences in transduction efficacies between AAV2 and AAV2.MC1 vectors at specific steps along the trafficking pathway.[37–39] HeLa cells were synchronized as described before. Thirty minutes post-transduction, AAV2 and AAV2.MC1 vectors were localized near the cell membrane as expected (Figure 5E). Bound AAV particles were evaluated by ddPCR detection of vector genomes. The results showed that cells treated with AAV2 vectors had 344.9 ± 35.6 gc/cell, while those treated with AAV2.MC1 vectors had 406.6 ± 28.1 gc/cell (Figure 5F). Although the difference was slight, it was statistically significant ($p < 0.05$). One hour post-treatment, 302.0 ± 25.1 gc/cell were detected to be internalized for the AAV2 vector-treated cells, while 374.2 ± 43.7 gc/cell were detected for cells treated with AAV2.MC1 vectors (Figure 5G). Since the MC1 modification was restricted to VP1u, cell surface binding and internalization of vectors were not anticipated to change with its inclusion. AAV2 is known to bind heparan sulfate proteoglycans (HSPGs).[40] We therefore aimed to evaluate whether binding to this receptor was altered by the MC1 modification. We compared the ability of AAV2 and AAV2.MC1 to be blocked by heparin (Figure S4). As predicted, we found that AAV2.MC1 was also blocked by heparin, while an AAV2 variant we identified previously to have lost affinity to heparin (AAV2.v66)[24] did not. Therefore, AAV2.MC1's ability to show a slight difference in binding and internalization is not through altered heparin sulfate binding and likely through another mechanism.

Around 4 h post-transduction, cells treated with AAV2 and AAV2.MC1 showed vector particles aggregated at the perinuclear space (Figure 5E). We observed that the colocalization of AAV capsids with the TGN was slightly higher in cells treated with AAV2.MC1 vectors (Figure 5E): ∼40% co-localization of A20 and TGN46 staining for AAV2.MC1 and ∼20% co-localization for AAV2 ($p < 0.01$; Figure 5H). Escape of AAVs into the cytoplasm is hypothesized to be dependent on VP1u's PLA_2 activity.[28] We therefore directly tested the PLA_2 activities of the AAV2 and AAV2.MC1 capsids. Interestingly, the PLA_2 enzymatic activity by AAV2.MC1 was 2-fold higher than the activity achieved by AAV2 (Figure 5I).

Figure 5. Characterization of MC1-modified AAV2 transduction kinetics

(A–D) Transduction of HeLa cells by sc*CB6-Egfp* vectors packaged with AAV2 or AAV2.MC1 throughout a 36-h period. (A) Representative epifluorescence images were captured at 36 h to show EGFP expression in cells transduced with AAV2 (top) and AAV2.MC1 (bottom) vectors. Scale bar: 0.5 mm). ddPCR was performed on cells harvested at the indicated time points post-transduction to measure the abundance of vector genomes (B) and *Egfp* transcripts (C). The abundance of transcripts per vector genome was also calculated for each time point (D), and linear regression values were determined ($n = 3$ for each time point). (E–H) HeLa cells were pre-chilled at 4°C for 30 min to synchronize endocytosis and transduced by the vectors. (E) Representative epifluorescence images of vector-transduced HeLa cells stained to visualize AAV capsids (A20, green), the *trans*-Golgi network (TGN46, red), and nuclei (DAPI, blue) 0.5 and 4 h post-transduction. Scale bar: 10 μm). (F) Cells were maintained at 4°C for 1 h, washed of unbound vector, and subjected to ddPCR to quantify binding of the vector. (G) Cells were incubated at 37°C for 1 h and harvested for ddPCR to quantify internalization of the vector. (H) Quantification of vector and TGN co-localization from images acquired from stained cells in (E) ($n = 5$ fields). (I) PLA_2 activity assessments of AAV2 and AAV2.MC1 ($n = 4$ trials). (J) Diagram illustrating the separation of cytoplasmic (gray) and nuclear (purple) fractions for vector genome quantification. (K) Percentage of vector genomes detected in cytoplasmic (gray) and nuclear (purple) fractions in cells treated with AAV2 or AAV2.MC1 vectors 4 and 6 h post-transduction. All values represent mean ± SD. $^*p < 0.05$, $^{**}p < 0.01$, $^{***}p < 0.001$, $^{****}p < 0.0001$ by unpaired *t* test.

Please cite this article in press as: Cui et al., Modification of the VP1u region boosts transduction of adeno-associated virus vectors for ocular gene therapy, Molecular Therapy (2026), https://doi.org/10.1016/j.ymthe.2026.01.029

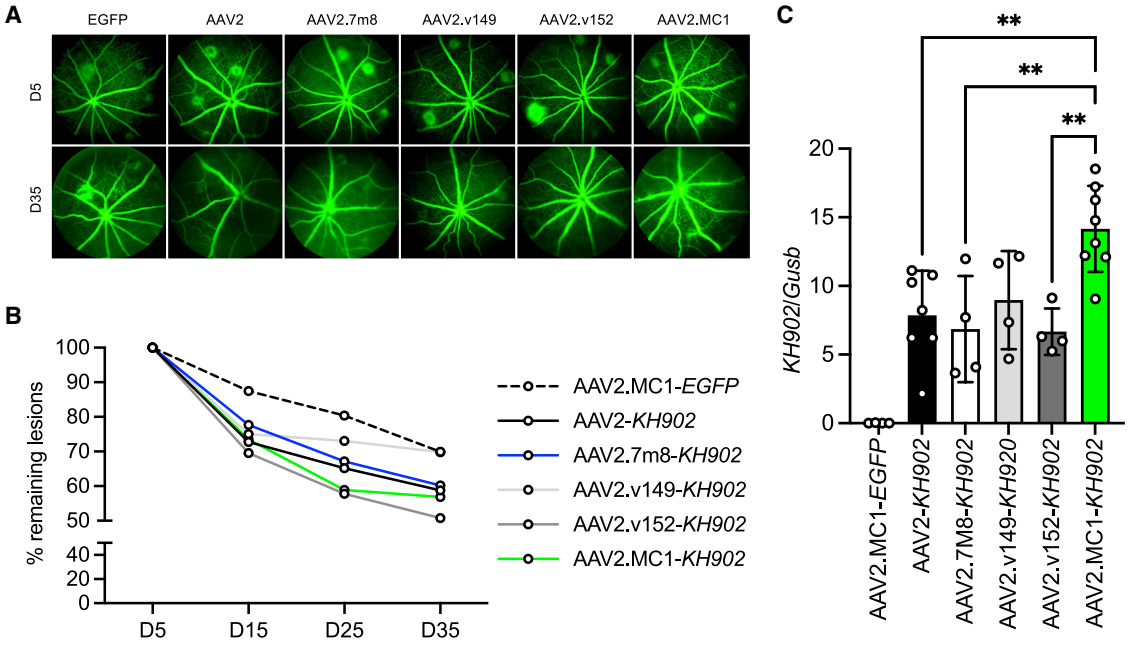

Figure 6. Treatment of CNV with AAV-vectored *KH902* packaged with test capsids

(A) Representative FFA images of mouse retinas 5 days (top row) and 35 days (bottom row) post-laser damage. Five days after laser damage, eyes were injected i.v.t. (1.5E9 vg/eye, 1 μL) with *ssCB6.PI.KH902* packaged with AAV2.7m8, AAV2.v149, AAV2.v152, or AAV2.MC1. (B) Quantification of the percentage of remaining leakage sites from the fifth day among treated eyes by the designated vectors 5, 15, 25, and 35 days post damage (AAV2.MC1-*Egfp*, AAV2.7m8, AAV2.v149, AAV2.v152, or AAV2.MC1). (C) Quantification of *KH902* transcripts in mouse retinas treated with the six test vectors. Values represent mean *KH902* levels normalized to *gusb* expression ± SD. $n \geq 4$. $^{**}p < 0.01$.

To gauge the kinetics of nuclear entry following transduction of HeLa cells between AAV2 and AAV2.MC1 vectors, we measured their genomes in nuclear and cytoplasmic fractions (Figure 5J). Western blots of nuclear and cytoplasmic fractions using antibodies against proteins found exclusively in the cytoplasm (vinculin) and the nucleus (laminA/C) were used to demonstrate contamination-free material (Figure S5). 4 h post-transduction, ∼30% of AAV2 vector genomes and ∼55% of AAV2.MC1 vector genomes were detected in the nucleus (Figure 5K). By six hours, both vectors exceeded 80% nuclear localization of vector genomes. These data indicate that AAV2.MC1 vector genomes were transported into the nucleus at a higher rate than those of the AAV2 vectors. It is notable to mention that the total abundance of vector genomes detected for AAV2.MC1-treated cells 4 h post-transduction had an ∼30% increase over AAV2-treated cells ($p < 0.05$) (Figure S6). This difference was marked by a 2.4-fold increase in the abundance of nuclear localized vector genomes in AAV2.MC1-treated cells compared to AAV2-treated cells ($p < 0.01$), while cytoplasmic fractions were similar. 6 h post-infection, both AAV2 and AAV2.MC1 vectors exhibited similar differences (Figure S6), suggesting that, although the percentage of nucleus-localized genomes may be equivalent by 6 h post-transduction (Figure 5K), the overall genomes were still greater for AAV2.MC1 (∼40% increase over AAV2 for total vector genomes and a 30% increase for vector genomes in the nuclear fraction).

Testing the therapeutic potential of rAAV2.MC1 delivering an anti-VEGF therapeutic transgene for treating choroidal neovascularization

To investigate whether the AAV2.MC1 capsid or the original AAV2 variants can be used to deliver a clinically relevant payload, we selected to package them with an anti-VEGF therapeutic transgene (*KH902*) driven by the *CMV* enhancer, chicken β-actin (CBA) hybrid promoter.[41] *KH902* is the transgene form of conbercept, an anti-VEGF recombinant protein under clinical investigation.[42,43] We tested the ability of the vectors to reverse choroidal neovascularization (CNV) in a laser damage C57BL/6 mouse model for wet AMD.[41,44–46] Five days after laser damage, mice were treated with the *KH902* vectors i.v.t.. We also tested AAV2 and AAV2.7m8 packaged with the *CBA-KH902* transgene for comparison. The AAV2.MC1.*Egfp* vector served as a negative control.

15 days post-damage (10 days post-vector treatment), eyes treated with the AAV2.MC1-*Egfp* control showed ∼87% remaining leakage sites (Figure 6B). Eyes receiving the *KH902* vectors showed ∼70%–78% remaining leakage sites, suggesting that the treatments can lower CNV in laser-damaged eyes. 25 days post-damage (20 days post-vector injection), eyes treated with AAV2.v149-*KH902* showed 73% remaining damage sites, while eyes treated with AAV2.7m8-*KH902* or AAV2-*KH902* showed ∼66% remaining damage sites, and eyes treated with AAV2.v152-*KH902* and AAV2.MC1-*KH902*

Please cite this article in press as: Cui et al., Modification of the VP1u region boosts transduction of adeno-associated virus vectors for ocular gene therapy, Molecular Therapy (2026), https://doi.org/10.1016/j.ymthe.2026.01.029

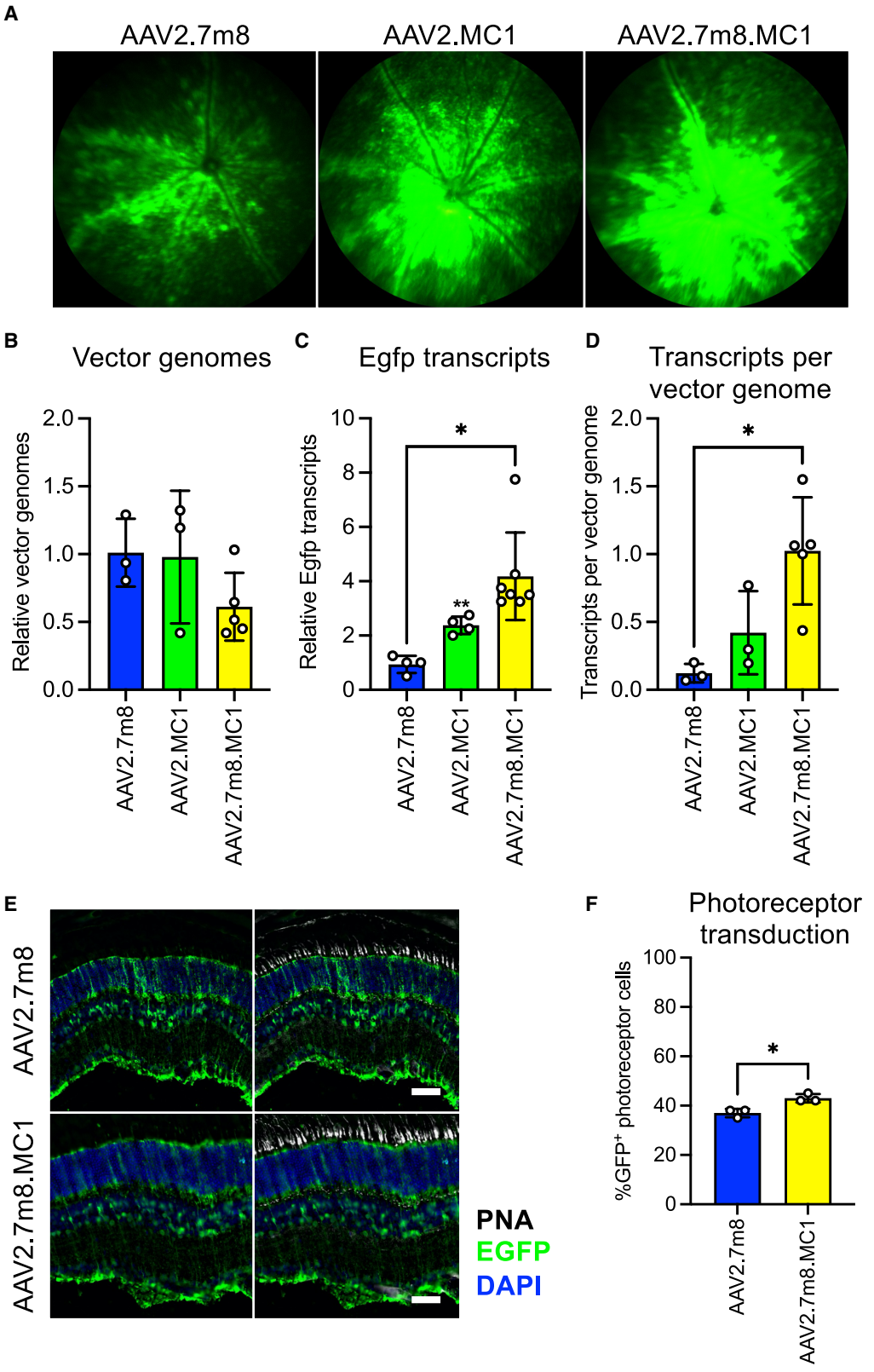

(legend on next page)

Please cite this article in press as: Cui et al., Modification of the VP1u region boosts transduction of adeno-associated virus vectors for ocular gene therapy, Molecular Therapy (2026), https://doi.org/10.1016/j.ymthe.2026.01.029

showed ~58% remaining damage sites. By 35 days post-damage (30 days post-vector injection), eyes treated with the negative control and AAV2.v145-*KH902* showed 70% remaining leakage sites. Eyes treated with AAV2 or AAV2.7m8 vectors showed ~60% remaining leakage sites, while those treated with AAV.MC1 vectors showed 57% of sites remaining. Eyes treated with AAV2.v152-*KH902* showed the lowest percentage of remaining damage sites (~51%) (Figure 6B).

After the 35-day time course, animals were sacrificed, and retinal tissues were harvested to measure *KH902* transcripts (Figure 6C). Tissues treated with AAV2.MC1-*KH902* exhibited the highest levels of *KH902* transcripts, nearly 2-fold greater than the detection of transcripts in retinas treated with either AAV2 or AAV2.7m8 vectors. It is unclear why the two variants did not result in relative increases in *KH902* transcripts after 35 days of treatment. Nevertheless, these results show that AAV2.MC1 has potential as a therapeutic transfer vehicle for treating retinal diseases.

The MC1 modification enhances the transduction profile of AAV2.7m8

Considering that the MC1 modification is on the VP1u domain of the capsid protein, we aimed to determine whether it could boost the transduction profile of AAV2.7m8. We grafted the MC1 residues onto the AAV2.7m8 capsid, and the resulting AAV2.7m8.MC1 capsid was evaluated for *Egfp* transduction by i.v.t. injection in mice. Funduscopy imaging of retinas 1 month post-treatment showed that the MC1 modification boosted AAV2.7m8 vector transduction (Figure 7A). Retinas were then harvested to analyze vector genome abundance (Figure 7B) and transcript levels (Figure 7C). We observed that the MC1 modification significantly increased transduction of the retina by nearly 10-fold, as assessed by transcripts per vector genome values (Figure 7D). Since the AAV2.7m8 capsid is known for photoreceptor transduction, we also gauged whether there was a general increase in photoreceptor transduction. Analyses of cryosections indicated that the MC1 modification slightly boosted EGFP expression in the outer segments (Figures 7E and 7F).

The MC1 modification boosts transduction of other serotypes in a context-dependent manner

We next aimed to determine whether the MC1 modification could increase the transduction profile of other serotypes. We selected to query whether AAV1, AAV3B, AAV8, AAV9, and AAV5, all clinically relevant serotypes,[16,47] can benefit from the MC1 modification. To this end, the VP1u region of each serotype was replaced with the entire VP1u region of AAV2.MC1. As before, capsids were packaged with sc*CB6.PI.Egfp*, and each was tested *in vitro* and *in vivo*.

We first evaluated the MC1-modified AAV1 capsid by transducing HeLa cells (Figures S7A–S7C). After 24 h, the AAV1.MC1 vector showed an approximate 2-fold greater transduction than achieved by the AAV1 vector (Figure S7C). In contrast, modification of AAV1 with the VP1u of AAV2 (VP1u2) did not significantly change the transduction profile of AAV1. Since AAV1 is known to be tropic to striated muscles, we tested the capacity of MC1 to increase skeletal muscle transduction. AAV1, AAV1.VP1u2, and AAV1.MC1 vectors were injected into mouse tibialis anterior (TA) muscles. One month after injection, we observed that AAV1.MC1 vectors resulted in higher EGFP expression than achieved by AAV1 vectors (Figure S7D). The MC1 modification conferred a 2-fold increase in transgene expression (Figure S7F).

We next evaluated grafting the MC1 modification onto AAV3B (AAV3B.MC1). Among the contemporary serotypes, AAV3B is the most similar to AAV2[26] and was therefore expected to also benefit from the MC1 modification. Transduction by AAV3B or by AAV3B.MC1 was first tested in HeLa cells. The MC1 modification led to double the percentage of transduced cells and nearly a 3-fold increase in mean fluorescence intensity (Figures S8A–S8C). AAV3B is also known to transduce human hepatocytes but not mouse hepatocytes.[48] We therefore opted to test the MC1-modified AAV3B capsid in cultured human hepatocytes (Huh7) but not in mouse hepatocytes *in vivo*. Transduction of Huh7 by AAV3B.MC1 led to a small but significant increase in the percentage of cells transduced when compared to AAV3B ($p < 0.01$) (Figures S8D and S8E) and a ~50% increase in mean fluorescence intensity by flow cytometry (Figure S8F).

Testing of the MC1 modification on AAV8 in HeLa cells resulted in a reduction in the percentage of transduced cells (Figures S9A and S9B). Interestingly, mean fluorescence intensities were equivalent in cells treated with the AAV8, AAV8.VP1u, and AAV8.MC1 vectors (Figure S9C), suggesting that overall vector trafficking and EGFP expression were not impacted by the MC1 modification—only cell entry was affected. AAV8 is best known for its tropism to the liver and muscle following systemic delivery. We therefore injected AAV8, AAV8.VP1u2, and AAV8.MC1 vectors into mice by tail vein administration. One month post-injection, we observed that the MC1 modification conferred a 2-fold increase in the transduction of TAs (Figures S9D–S9F), while liver transduction by AAV8.MC1 vectors was not significantly different from the transduction achieved by AAV8 vectors (Figures S9G–S9I). Interestingly, AAV8.MC1 vectors showed a non-statistically significant increase in vector genomes in the TA (Figure S9E) but a significant decrease in the liver (Figure S9H). These results indicate that the MC1 modification may confer context-dependent benefits.

Figure 7. The MC1 modification enhances AAV2.7m8 *in vivo* transduction

(A) Fluorescence funduscopy of representative mouse eyes 1 month post-i.v.t. delivery of scCB6.*Egfp* vectors packaged with AAV2.7m8, AAV2.MC1, or AAV2.7m8.MC1. (B–D) Quantification of relative vector genomes (B), *egfp* transcripts (C), and transcripts per vector genomes (D) from treated eyes 1 month post injection. $n \geq 3$. (E) Retinal cross-sections stained to visualize photoreceptors (PNA, white), EGFP (green), and DNA (DAPI, blue). Scale bar: 500 μm.
(F) The percentage of EGFP-positive photoreceptor cells. $p < 0.05$, $n = 3$.

Please cite this article in press as: Cui et al., Modification of the VP1u region boosts transduction of adeno-associated virus vectors for ocular gene therapy, Molecular Therapy (2026), https://doi.org/10.1016/j.ymthe.2026.01.029

Both AAV9 and AAV9 modified with MC1 (AAV9.MC1) showed poor transduction of HeLa cells (Figures S10A and S10B). Nevertheless, modification of AAV9 with MC1 led to a greater than 75% decrease in the percentage of transduced cells and an ∼50% decrease in EGFP expression (Figure S10B). Interestingly, grafting VP1u2 onto AAV9 led to a drastic decrease in the percentage of transduced cells, but this decrease did not influence EGFP expression (Figure S10B). This outcome suggests that VP1u2 altered the cell entry of AAV9 but not transgene expression. AAV9 is best known for its ability to traverse the blood-brain barrier to transduce cells of the CNS. AAV9 can also transduce a range of tissues, including liver and muscle. We injected neonatal mice with test vectors to assess whether MC1 enhances AAV9 vector transduction in the brain, liver, and skeletal muscle. One month post-injection, EGFP expression was not detected in tissues treated with AAV9.MC1 vectors by cryosection and epifluorescence microscopy (data not shown). Importantly, ddPCR analyses confirmed no difference in transduction between AAV9 and AAV9.MC1 vectors in the brain or liver (Figures S10C and S10D). Notably, the VP1u2 modification of AAV9 increased brain transduction ∼2-fold (Figure S10C). AAV9.MC1 vectors showed a 75% decrease in the transduction of TAs compared to what was achieved by AAV9 vectors (Figure S10E). Additionally, modification of AAV9 with VP1u2 also led to a slight decrease in transduction. Again, this outcome suggests a context-dependent effect of VP1u function.

The AAV5.VP1u2 and AAV5.MC1 vectors showed a more than 2-fold increase in transduction of HeLa cells than what was achieved by the AAV5 vectors (Figures S11A–S11C). Although this outcome demonstrates that the MC1 modification can boost AAV5 transduction, the impact may be exerted by the other VP1u2 residues. This concept is certainly supported by the AAV2.5T capsid, which is a chimeric capsid that harbors the N-terminus of AAV2 (amino acids [aa] 1–128) and the C-terminus of AAV5 (aa 129–725).[49] The AAV2.5T capsid can strongly transduce human airway epithelial (HAE) cells.[49] We therefore evaluated the function of the MC1 modification on AAV2.5T. We tested AAV2.5T.MC1 transduction in HeLa and A549 cells (human lung cancer epithelial cells)[50] and found that the MC1 modification can modestly but significantly boost AAV2.5T transduction (Figures S11D–S11I). To assess *in vivo* performance, we delivered AAV2.5T.MC1 and AAV2.5T vectors into mice via the tail vein. One month post-injection, AAV2.5T.MC1 vectors showed slightly stronger liver transduction than conferred by AAV2.5T vectors, but no difference in the lungs was observed (Figures S11J and S11N). In support of this observation, ddPCR assays showed 2-fold greater transduction of livers and lungs than what was achieved by AAV2.5T vectors (Figures S11L and S11P). However, transcripts per vector genome values were not significantly different between treatment groups (Figures S11M and S11Q).

DISCUSSION

Current capsid engineering efforts have primarily focused on modifications of VP3, especially within VR-IV and VR-VIII, which are the outermost protruding domains of the AAV capsid. These regions contribute to the 3-fold spike domain of the assembled capsid and are believed to be the principal determinants of serotype tropism. In our discovery of natural AAV2 variants, we found that 26% had packaging yields that were equivalent to or better than AAV2. We chose to only focus on these capsids to screen *in vivo*, potentially ruling out variants that may exhibit favorable transduction profiles. However, if a capsid shows ideal transduction efficacy but is difficult to produce, it would not be a viable capsid for clinical use. Additionally, AAV2 is known to be a poorer producer compared to other serotypes[51]; thus, a variant that yields lower titers than AAV2 would be less than ideal.

Through our screen of variants in the retina, we unexpectedly found that the only candidates that strongly transduced retinal tissues were those that shared all VP3 residues with AAV2. One key aspect of AAV2 is its ability to bind HSPG, which has been presumed to be a result of cell culture selection.[52] Since our capsids were derived from natural variants identified from proviral sequences in human tissues, the presence of multiple AAV2 variants identified in our screen that retain the necessary HSPG binding residues (R585 and R588) challenges this premise. Another key outcome of this investigation was that the variant residues of the top-performing capsids in our screen were those found within VP1u (E36G D80N, and V125A). To date, the function of VP1u remains understudied, since it is not presumed to play any role for cell surface receptor binding or serum factor binding, including antibodies.

By combining the three defining residues among the discovered variants into a single capsid, we engineered a novel VP1u modification that can boost overall vector transduction through enhanced intracellular trafficking (Figure 6). We did find that AAV2.MC1 showed a marginal but significant increase in cell binding and internalization. Although the mechanism of altered binding was not determined in this study, we did show that the MC1 modification did not alter AAV2's binding to heparin (Figure S4). Nevertheless, improvements to post-entry steps are the main driving force underpinning the ability of the MC1 modification to improve AAV2 vector transduction. These improvements may increase overall transcript expression, since rAAVs that do not escape from LEs are degraded in the lysosome, when they fuse with lysosomes.[36,39,53]

Two of three amino acids that define MC1 are situated at the PLA_2 domain (D80N) and near the BR1 region (V125A) (Figure S2). Whether increasing PLA_2 activity necessarily improves transduction is not entirely clear. A recent study has shown that swapping parvoviral PLA_2 domains onto AAV9 resulted in functional improvement.[54] We also showed that the MC1 modification led to increases in nuclear entry kinetics, since AAV2.MC1 showed a higher percentage of nuclear-localized vector genomes than what was achieved by AAV2 4 h post-transduction of cells in culture (Figure 5K). Increased nuclear localization kinetics will no doubt result in improvements to transduction, but it should also be noted that the differences in transduction persist beyond the 4- to 6-h time period assayed in these

Please cite this article in press as: Cui et al., Modification of the VP1u region boosts transduction of adeno-associated virus vectors for ocular gene therapy, Molecular Therapy (2026), https://doi.org/10.1016/j.ymthe.2026.01.029

experiments (Figures 5B–5D). This finding suggests that faster nuclear entry kinetics are not the sole reason for AAV2.MC1's improvements over AAV2, since transcript levels conferred by AAV2 do not "catch up" to levels achieved by AAV2.MC1. Sustained improvements to *in vivo* transduction by MC1 1 month post-treatment support this notion (Figures 3, 4, 6, 7, and S7–S11).

The third amino acid modification within VP1u (E36G) is located in a region with no clear function. A recent report suggests that the N-terminal sequence of AAV8 VP1u (aa 1–53) is involved in transcriptional regulation.[33] The increases in transcripts per vector genome values resulting from the MC1 modification certainly suggest that it may impact transcriptional activation (Figures 5D and 7D). Further investigations of whether E36G or other N-terminal residues can improve transduction through post-nuclear entry mechanisms are warranted.

Importantly, our work has shown that the MC1 modification can boost AAV2 transduction of the mouse retina (Figure 3). This improvement even surpassed the transduction profile of AAV2.7m8, which is currently being used in a gene therapy trial for wet AMD.[21] This AAV2.7m8-based gene therapy, called ixoberogene soroparvovec, is an i.v.t. delivery of the anti-VEGF protein therapy aflibercept. Unfortunately, it has been shown to elicit host immune responses and vasculitis.[55] We have previously demonstrated that AAV2.7m8 vectors have a higher penchant for packaging truncated genomes.[22] Knowing that alternatives to AAV2.7m8 are needed, the MC1 modality represents a possible capsid alternative for retinal disease gene therapy. We note that the AAV2.MC1 capsid transduced photoreceptor cells as well as AAV2.7m8 by counting outer segments (Figure 3K). However, one caveat is that a proper reporter mouse line, such as the neural retina leucine zipper (*NRL*)-*GFP* line,[56] would be a more accurate *in vivo* model for assessing photoreceptor transduction.

We were able to show that the MC1 modification can boost AAV2.7m8 transduction in mice (Figure 7), suggesting that the modification can potentially be applied to any retinal-tropic capsid that is developed. Remarkably, the VP1u graft can also benefit other serotypes (Figures S7–S11). However, our findings showed that functional improvement by MC1 modification is context dependent and suggest that intracellular trafficking profiles for AAV transduction are not conserved in all cell types. Although we do not have a clear mechanism to explain this context difference, it is plausible that VP1u may interact with cell-type-specific proteins that can impact intracellular trafficking kinetics. These proteins may also interact with known factors that mediate AAV retrograde trafficking, such as the Golgi/TGN-resident cellular receptors AAVR[36] and GPR108.[57] Another intriguing possibility is that the MC1 modification exerts transcriptional activity on the transgene promoter. The concept that the AAV capsid can impact transcriptional activity is relatively new,[33,58] and the contribution of VP1u toward species- or cell-type-specific transcription is in line with current findings by others.[33]

Although our current experimental support is limited to a few animals and the EGFP expression was variable between the two samples for both AAV2.7m8 and AAV2.MC1 vector-treated retinas, the AAV2.MC1 capsid was shown to be superior to AAV2 in conferring transduction of canine and NHP retinas following i.v.t. injections (Figures 4 and S3). We note that our results stemming from mouse, canine, and our single NHP study show drastically different transduction outcomes. These apparent inconsistencies are likely due to differences with inner limiting membranes, vitreous volumes, cell surface proteins, and intracellular factors between diverse species. These factors can alter transduction profiles and can complicate how translatable a capsid is for clinical use.[59] Further work in these large-animal models is needed to substantiate our findings and to lend support toward using the AAV2.MC1 capsid as a viable retinal gene therapy vehicle. Nevertheless, we have shown that AAV2.MC1 can package and deliver an anti-VEGF therapeutic transgene to treat CNV (Figure 6). Since AAV2.MC1 shows improvements in transduction across several retinal layers and cell types, including ganglion cells, bipolar cells, photoreceptors, and RPE cells (Figures 3 and 4), it has the potential to benefit therapies for glaucoma, LHON, retinitis pigmentosa, Stargardt disease, RPE65-associated inherited retinal dystrophy, and others.[11–15]

In summary, our findings show that VP1u region modifications derived from natural amino acid variants of AAV2 can increase capsid transduction through improvements of intracellular trafficking kinetics in a context- and serotype-dependent manner. Our results also highlight VP1u as a critical modulator of AAV vector transduction, offer insights into AAV intracellular trafficking kinetics, and provide new avenues for designing next-generation capsids.

MATERIALS AND METHODS

Clinical sample collection and NGS

The methods for genomic DNA extraction for the identification of proviral AAV *cap* sequences from human tissues have been described previously.[24,34] In brief, samples were stored in liquid nitrogen until DNA extraction. To avoid AAV DNA cross-contamination, DNA extraction and PCR procedures were performed in a sterile UV-irradiated biosafety cabinet. All surfaces and equipment were sprayed with DNA-Exitus Plus (Applichem, A7089) and wiped clean with Milli-Q water after 15 min. Frozen tissues were then thawed at room temperature, quickly cut to about 25 mg of tissue with disposable scalpels, and placed in a 2 mL tube. Extraction of DNA from tissues was performed using the QIAamp DNA Mini Kit (QIAGEN, 51306) according to the manufacturer's recommended procedures.

For long-read SMRT sequencing and bioinformatics, amplicon libraries were generated from genomic DNA by standard PCR procedures. To amplify AAV genomes, PCR was performed using Platinum PCR SuperMix High Fidelity (Invitrogen) with the following cycle conditions: 97°C for 1 min; 46 cycles of 98°C for 10 s, 60°C for 15 s, and 68°C for 2 min 30 s; and 68°C for 10 min. Correctly sized PCR products were gel purified with a PureLink PCR Purification Kit

(Thermo Fisher Scientific) and used for a second round of 15-cycle PCR for barcoding. The primer pairs used were as follows:

First-round primers:

CapF: 5′-GACTGCATCTTTGAACAATAAATGA-3′

CapR: 5′-GAAACGAATTAACCGGTTTATTGATTAA-3′

Second-round primers:

EF: 5′-CATCACTACGCTAGATGACTGCATCTTTGAACAA TAAATGA-3′

ER: 5′-TAGTATATCGAGACTCGAAACGAATTAACCGGTT TATTGATTAA-3′

Amplicon SMRT sequencing of AAV *cap* ORFs and downstream bioinformatics pipelines were performed as described previously.[24] Standard SMRT sequencing libraries were generated by the UMass Chan Medical School Deep Sequencing Core (DeepSeq Core). Sequencing was performed on the RSII platform. SMRT sequencing reads were mapped to the AAV2 *cap* ORF using the Burrows-Wheeler aligner-maximum exact matches (BWA-MEM) algorithm.[60] Reads were processed through InDelFixer (https://github.com/cbg-ethz/InDelFixer) to remove single-nucleotide insertions and deletions that may result from error-prone PCR or sequencing errors, and *de novo* assembled using Geneious R9 to cluster reads with 99% of sequence similarity. Only read clusters represented by at least 10 reads were considered unique DNA capsid sequences. DNA sequences were then translated to amino acid sequences to define the final list of unique AAV2 variant capsids.

Plasmid constructs and vector production

AAV2 variants and barcoded Egfp *transgenes*

The AAV2 variant capsid ORFs were synthesized and cloned into the pAAV2/8 *trans* plasmid (provided by the UMass Chan Viral Vector Core) by Applied Biological Materials (Richmond BC, CAN). We designed a strategy for the detection of barcoded EGFP transcripts, whereby an 8-nt barcode (95 unique barcodes) was inserted into the 3′ UTR of the self-complementary vector plasmid containing the ubiquitously expressed EGFP reporter gene (UMass Chan Viral Vector Core). A list of the barcodes used and their corresponding capsid variants are provided in File S1. The resulting *Egfp-bc* transgene is expressed by the *CMV* enhancer, CBA hybrid promoter (*CB6*). Large-scale, endotoxin-free (<100 EU/mg) AAV2 variant *trans* plasmids, barcoded *cis* plasmids, and the helper plasmid (pAd-DeltaF6) were generated by Synbio Technologies (Mammoth Junction, NJ, USA). Vectors were purified by CsCl gradient ultracentrifugation as a pool. The resulting library titer was 9.76E12 vg/mL.

VP1u-related capsid trans *plasmids*

To generate the mutant VP1u capsid *trans* plasmids, site-directed mutagenesis was employed using KOD (*T. kodakaraensis* KOD1) polymerase and 2× HIFI Master (New England Biolabs) and primer sets detailed in Table S1 (Integrated DNA Technologies [IDT]).

All plasmid preparations were quantified by fluorometry (Qubit, Thermo Fisher Scientific) and checked by Sanger sequencing or nanopore sequencing (PlasmidEZ, Azenta/Genewiz).

Viral vector production and purification

Vectors used in this study were produced using the triple-plasmid transfection method in HEK293 cells.[61] Crude lysates were obtained from small-scale production in HEK293 cells. After 3 days of culturing, cell lysates were subjected to three freeze-thaw cycles. Cell debris was removed by centrifugation, and supernatants were used for the titration of vectors. Select vectors were also purified by CsCl gradient ultracentrifugation as described previously.[61] Vectors were aliquoted into 200 μL stock and stored at −80°C immediately after production. Thawed aliquots were kept at 4°C before use and warmed to room temperature before injection.

The titrations reported in this study were performed by ddPCR using probes against *Egfp* (Thermo Fisher Scientific, Mr04329676_mr) or *nRGB* (Forward: GCCAAA AATTATGGGGACAT, Reverse: ATTCCAACACACTATTGCAATG, and TaqMan probe: 6-carboxyfluorescein (6FAM)-ATGAAGCCCCTTGAGCATCTGACTTCT-tetramethylrhodamine [TAMRA]). Probes and primers were synthesized by IDT.

Animals

All animal procedures described in this study were approved by the UMass Chan Medical School or Michigan State University institutional animal care and use committees.

Mice

Four- to six-week-old female C57BL/6J mice were purchased from The Jackson Laboratory. Mice were kept on a 12 h light/12 h dark cycle at 70°F–74°F with 35%–46% humidity for the entirety of the studies. Mice were fed normal chow (ISO-pro 300 Irradiated Diet, 5P76).

Injections by s.r. and i.v.t. were performed with glass needles (Clunbury Scientific, B100-58-50) to deliver ∼1 μL of fluid into the subretinal space or vitreous using a FemtoJet (Eppendorf) with a constant pressure of 300 psi and an injection time of 1.5 s. For the variant library screen, a total of 3.0E9 vg/eye was injected (n = 3). Specific doses for other experiments are described under results. EGFP expression in mouse retinas was observed by fluorescence funduscopy (Phoenix MICRON IV retinal imaging microscope) 4 weeks post-injection. One month after injections, mouse retinas were harvested and subjected to DNA and RNA extraction. Bulk RNA was subjected to target-specific (*Egfp-bc*) reverse transcription. Genomic material was subjected to amplicon sequencing.

Laser damage model for CNV

Laser damage was performed at 2 months of age as previously described.[41] To determine how well CNV was induced, we

performed fundus fluorescein angiography (FFA) 5 days post-damage to establish the total number of successful leakage sites (indication of neovascularization), as not all initial damage sites produced sufficient injury to Bruch's membrane to produce neovascular pathology. The number of leakage sites recorded on day 5 for each vector represented the denominator for the percentage calculation of remaining leakage sites over time. On the fifth day, mice were injected i.v.t. with the *KH902* vectors. After vector treatment, FFA images were taken every 10th day until 35 days post damage, and the remaining leakage sites were counted. Eyes treated with the AAV2.MC1-*Egfp* control served as the benchmark for natural healing of damaged sites.

Histology

Imaging of cryosections and flat mounts were performed as previously described.[41] For flat mounts, retinas were separated from the eye cup before fixation in 4% paraformaldehyde (PFA) and cut with equidistant radial incisions from the optic disc to generate a four-leaf structure. For cryosections, select eyecups were dissected in cold 1× PBS and fixed in 4% PFA overnight at 4°C. Cryosections were cut at a thickness of 12 μm. The following primary antibodies and dilutions were used: chicken anti-EGFP antibody (1:1,000 dilution; Abcam, ab13970) and rabbit anti-IBA1 (1:300 dilution; Wako, 019-19741). The chromophore conjugate fluorescein peanut agglutinin lectin (PNA) (1:500 dilution; Vector Laboratories, FL1071) was used to stain cone photoreceptors. The anti-BRN3A antibody (1:250 dilution; Abcam, ab245230), CHX10 antibody (1:1,000 dilution; Santa Cruz Biotechnology, sc-365519), anti-PROX1 antibody (1:1,000 dilution; Abcam, ab199359), and LIM1 polyclonal antibody (1:1,000 dilution; Thermo Fisher Scientific, PA5-116485) were used to stain ganglion cells, bipolar cells, amacrine cell, and horizontal cells, respectively. All antibodies were diluted in PBS with 0.3% Triton X-100 and 5% bovine serum albumin (Cell Signaling Technology). Nuclei were counterstained with DAPI (1:2,000 dilution; Santa Cruz Biotechnology, CAS 28718-90-3). All secondary antibodies were purchased from Thermo Fisher Scientific. Sections were mounted in Fluoromount-G mounting medium (Southern Biotech, 0100-01). All images were visualized with a Leica DM6 Thunder microscope with a 16-bit monochrome camera. Images were processed by LAS X Life Science microscope software.

Tail vein injections

Intravenous (i.v.) injections were performed at a volume of 150 μL and at a dose of 1E11 vg/mouse. 30 days post injection, mice were sacrificed for tissue collection. Tissue samples (liver, lungs, and skeletal muscles) were fixed and mounted in Optimal Cutting Temperature (OCT) compound or ground into powder in liquid nitrogen and stored at −80°C. Tissues mounted in OCT were cryosectioned at a thickness of 12 μm. Images were visualized using epifluorescence microscopy (Leica DM6 Thunder and LAS X Life Science).

NHPs

Cynomolgus macaques were screened for neutralizing antibodies against AAV2 to ensure that dosing of vectors would not elicit immune responses to the capsids. Animals with a neutralizing antibody titer of 50% (NAb_{50}) dilution <1:10 were selected for the study. Animals were administered the vector at the designated doses. Injections for the single animal described in Figure S3 were performed with assistance from Biomere (Worcester, MA, USA). One month post-injection, animals were euthanized, and retinal tissues were harvested for cryosectioning and molecular analyses. 12-μm cryosections were stained with PNA, anti-EGFP primary antibody with goat anti-chicken Alexa Fluor 488 secondary antibody, and DAPI. Sections were mounted as described before. Images were acquired using the Leica DM6 Thunder microscope and LAS X software.

Canines

Wild-type adult beagles were injected with 1E10 vg/eye of vector in 170 μL. Fundus autofluorescence images were taken 1 month post injection, and then the animals were euthanized. Retinal tissues were harvested, cryosectioned, stained, and imaged.

Amplicon sequencing of barcoded Egfp transgenes

Nucleic acid (DNA and RNA) purification of mouse or NHP retinal tissues was performed using the RNA/DNA/Protein Purification Plus Kit (Norgene Biotex, 47700). Bulk RNA was reverse transcribed using target-specific primers (Table S2) and iScript Reverse Transcription Supermix (Bio-Rad, 170-8840) following the manufacturer's recommended procedures. We then PCR amplified the 8-nt barcode region using primer sets that contained secondary barcodes to differentiate between seven sample groups: 3 RNA, 3 DNA, and 1 vector input (Table S2). Amplicons were then subjected to Illumina sequencing (Hiseq 3000) by the UMass Chan Deep Sequencing Core following the manufacturer's recommended procedures. The resulting reads were processed by custom workflows on Galaxy[62] to tabulate the abundance of barcodes detected within each sample. In brief, quantification of barcodes detected in tissues was normalized over the detection of barcodes in the vector input and then scaled to the detection of vector genomes or transcripts attributed to AAV2, set to 100 (File S1).

Cell culture

rAAV transduction assays

HeLa cells were seeded in 10% FBS in DMEM (Life Technologies, 11965126) at a density of 4E4 cells/well in a 24-well plate and incubated in a 37°C, 5% CO_2 incubator overnight. After 16 h, cells were co-infected with 10 μL/well of HEK293 crude lysates with AAV vectors or purified rAAVs at an MOI of 5E3 to 2.5E4 vg/cell and adenovirus serotype 5 (AdV5) at an MOI of 100 vg/cell. 24–48 h post-infection, cells were subjected to epifluorescence imaging to capture EGFP expression. Cells were trypsinized and collected after imaging and subjected to flow cytometry on an Attune NxT cytometer (Thermo Fisher Scientific) or DNA and RNA isolation by an Allprep kit (QIAGEN) to measure transduction.

Synchronized transduction and AAV trafficking assays

rAAV binding and internalization assays were performed as previously reported.[63] In brief, HeLa cells were seeded in 12-well plates

Please cite this article in press as: Cui et al., Modification of the VP1u region boosts transduction of adeno-associated virus vectors for ocular gene therapy, Molecular Therapy (2026), https://doi.org/10.1016/j.ymthe.2026.01.029

with 5E4 cells/well 1 day before transduction. Cells were pre-chilled at 4°C for 1 h to halt endocytosis. Cells were then transduced with AAV vectors diluted in 50 μL of PBS to achieve an MOI of 1E5 vg per cell and incubated at 4°C for another hour. After incubation, cells were washed with ice-cold Dulbecco's PBS (DPBS; Corning, 21-031-CV) three times to remove unbound rAAVs and replaced with complete culture medium. Cells were then moved to a 37°C incubator. At this stage, the timepoint was set as "0 h" for epifluorescence imaging (Leica) or harvested. To quantify vector binding, cells were harvested 15 min post-transduction and subjected to total DNA isolation using a QIAamp DNA Mini Kit (QIAGEN, 51304). To quantify internalization of vectors, cells were incubated at 37°C in complete culture medium in 5% CO_2 for 1 h. After incubation, cells were detached with enzyme cell detachment medium (Accutase, Thermo Fisher Scientific, 00-4555-56) for 10 min at 37°C, followed by quenching with complete culture medium. Cells were gently pelleted at 2,000 rpm for 2 min at room temperature and washed with DPBS three times, followed by total DNA isolation as described above. Samples were then collected at different time points (4–36 h) as described in the text and gently pelleted. Nucleic acids (DNA and RNA) from whole cells were isolated using the RNA/DNA/Protein Purification Plus Kit (Norgene Biotex, 47700) following the manufacturer's recommendations. Bulk RNA was reverse transcribed into a cDNA library with an iScript Reverse Transcription Supermix Kit (Bio-Rad, 170-8840) following the manufacturer's recommended procedures. Genomic DNA (gDNA) and cDNA were subjected to ddPCR using probe sets specific to *Egfp* (Table S3) to quantify rAAV DNA distribution and *egfp* expression. Probes against *RNaseP* or *HPRT1* were used as housekeeping genes for gDNA and cDNA samples, respectively, to calculate relative AAV vector and transgene abundance.

TGN staining and imaging

HeLa cells were seeded at 4E4 cells per well onto poly-D-lysine/laminin-coated 12 mm glass coverslips (Corning) in 24-well plates and incubated overnight. After 16 h, cells were moved to 4°C to pre-chill for 1 h. Cells were then infected with AAV2 or AAV2.MC1 vectors at an MOI of 1E5 vg/cell and incubated at 4°C for another hour. Cells were then washed three times with cold PBS to remove unbound vectors, fresh culture medium was added, and cells were incubated at 37°C. After 0.5 or 4 h, cells were fixed with 4% PFA, washed three times with PBS, and permeabilized with 0.25% Triton X-100 diluted in PBS at room temperature for 1 h. Cells were incubated for 1 h at room temperature in blocking buffer (5% goat serum [Invitrogen, 50062Z] and 0.25% Triton X-100 diluted in PBS). Cells were then incubated with primary antibodies, anti-TGN46, Abcam, ab50595 (1:500); or A20, Progen, Cat 61055 (1:200) diluted in blocking buffer. Cells were then washed three times in PBS and incubated for another hour in DAPI and fluorescently tagged secondary antibodies (Alexa Fluor 488 anti-mouse and Alexa Fluor 594 anti-rabbit, 1:1,000 dilutions, Thermo Fisher Scientific). Cells were washed a final three times in PBS, and coverslips were mounted onto glass slides. Cells were visualized and images acquired using a Leica SP8 confocal microscope.

Subcellular fractionation assays

Subcellular fractionation was achieved by following the method described at https://www.abcam.com/en-us/technical-resources/protocols/subcellular-fractionation with slight modifications. Briefly, cells were detached by scraping in 500 μL ice-cold fractionation buffer. Each cell sample was then lysed by passing through a 27G needle 10 times and set on ice for 10 min. These two steps were then repeated. The samples were then pelleted by centrifugation at 720 × *g* for 5 min. Supernatants were centrifuged again to fully remove nuclei. Supernatants from the top 250 μL of the second spin were aliquoted as clean cytoplasm fractions. Pellets (nuclear fractions) were resuspended in 500 μL fractionation buffer. Pellets were dispersed by passing through a 25G needle 10 times and incubated on ice for 10 min. Pellets were centrifuged again at 720 × g for 10 min, and the supernatants were discarded. Pellets were resuspended and centrifuged again to fully remove cytoplasmic contamination. The remaining clean nuclei were resuspended in 50 μL of fractionation buffer.

To validate the purity of nuclear versus cytoplasmic cell fractions, Western blotting was performed. Briefly, 10 μL of cell lysates were loaded onto an SDS polyacrylamide gel and resolved. Proteins were transferred onto nitrocellulose membranes and stained with anti-vinculin (1:1,000 dilution; Abcam, ab219649) and anti-lamin A/C antibody (1:1,000 dilution; Santa Cruz, sc-376248). The IRDye 680RD donkey anti-mouse immunoglobulin G (IgG) secondary antibody (1:2,000 dilution, LI-COR Biosciences) and IRDye 800CW goat anti-rabbit IgG secondary antibody (1:2,000 dilution, LI-COR Biosciences) were used. Blots were imaged using a LI-COR Biosciences Odyssey M instrument.

The nucleic acids from cytoplasmic and nuclear fractions were isolated using an RNA/DNA/Protein Purification Plus Kit (Norgene Biotex, 47700) following the manufacturer's recommendations. Both fractions were subjected to ddPCR to quantify rAAV DNA distribution. Vector gDNA was detected using a probe set against *Egfp* (Table S3). Samples were also probed for *RNaseP* and mtDNA-tRNA^{Leu} (forward primer: CACCCAAGAACAGGGTTTGT; reverse primer: TGGCCATGGGTATGTTGTTA; probe:/5HEX/TTACCGGGC/ZEN/TCTGCCATCT/3IABkFQ/; Integrated DNA Technologies)[64] to verify the purity of nuclear and cytoplasmic fractions, respectively.

Quantification of vector genomes and transcripts by ddPCR

The concentrations of isolated DNA and reverse-transcribed cDNA samples from animal tissues or cells were measured by absorbance at 260 nm (Nanodrop). 10–20 ng of DNA sample or approximately 10–100 ng of cDNA was processed for ddPCR reactions. Probes for targeting *Egfp*, transferrin receptor (*Tfrc*), and beta-glucuronidase (*gusb*) are summarized in Table S3. ddPCR droplets were generated in the QX100/200 Droplet Generator (Bio-Rad) using droplet generation oil following the manufacturer's instructions. The ddPCR mix was amplified following the Supermix (Bio-Rad, 1863024) protocol. The ddPCR mix was assayed in a QX200 reader (Bio-Rad), and the results were analyzed using the QuantaSoft software.

PLA_2 activity assay

Purified vectors were subjected to 70°C heating for 15 min to externalize the VPu1 domains and then assayed for PLA_2 enzymatic activity using the Secretory Phospholipase A2 Assay Kit (Abcam, ab133089) following the manufacturer's recommended procedures.

Statistical analysis

One-way or two-way ANOVA with Tukey's method for multiple comparisons was used as indicated. $p < 0.05$ was considered statistically significant and plotted accordingly.

DATA AND CODE AVAILABILITY

All raw NGS (long-read and short-read) datasets will be made available upon request.

ACKNOWLEDGMENTS

G.G. is supported by grants from UMass Chan Medical School (an internal grant) and by the National Institutes of Health (R01NS076991-01, P01HL131471–05, R01AI121135, UG3HL147367–01, R01HL097088, R01HL152723–02, U19AI149646-01, and UH3HL147367-04). P.W.L.T. is supported by The National Institutes of Health (1R21AI183080-01A1), an award from The Bassick Family Foundation, and a BRIDGE Fund Award (a UMass Chan Medical School internal grant). We would like to extend our thanks to Dr. Elisabet Mandon, Dr. Sandhiya Ravi, Dr. Manish Muhuri, Dr. Yukiko Maeda, Dr. Jiaming Wang, and Dr. Hao Chang for generous help, guidance, technical training, and suggestions. We would also like to thank the UMass Chan Deep Sequencing core (Dr. Maria Zapp, Dr. Daniella Wilmot, and Dr. Ellie Kittler), Microscopy core (Dr. Christina Baer), and Morphology core (Dr. Yu Liu) for help with sample preparation, data processing, and technical support.

AUTHOR CONTRIBUTIONS

M.C., G.G., P.W.L.T., C.P., A.M.R., and M.S.G.-K. conceived and designed the study. Q.S. and J.X. generated the AAV vectors described in the study. M.C., S.-Y.C., J.L., J.M., X.C., M.X., G.X., L.L., J.W., F.Z., M.Y., B.R., C.D.H., A.L.J., L.E.K., M.A.M., S.N., T.S., T.B.L., W.B., A.L., X.C., T.X., M.S.G.-K., and A.K. acquired the data. M.C., G.G., C.P., D.W., Y.W., A.M.R., S.C., B.T., H.L., and P.W.L.T. analyzed and interpreted the results. M.C., C.P., A.M.R., M.S.G.-K, A.K., and P.W.L.T. drafted and revised the manuscript. G.G. and P.W.L.T. approved and finalized the manuscript. All authors have agreed to be accountable for all aspects of the work by ensuring that questions related to the accuracy or integrity of any part of the work are appropriately investigated and resolved.

DECLARATION OF INTERESTS

G.G. is a scientific co-founder of Voyager Therapeutics and Aspa Therapeutics and holds equity in these companies. G.G. and P.W.L.T. are inventors on patents with royalties licensed to biopharmaceutical companies. G.G., C.P., and P.W.L.T. also received sponsored research support from Kanghong Pharmaceuticals for unrelated research. The remaining authors declare no competing interests.

SUPPLEMENTAL INFORMATION

Supplemental information can be found online at https://doi.org/10.1016/j.ymthe.2026.01.029.

REFERENCES

1. Wang, D., Tai, P.W.L., and Gao, G. (2019). Adeno-associated virus vector as a platform for gene therapy delivery. Nat. Rev. Drug Discov. *18*, 358–378. https://doi.org/10.1038/s41573-019-0012-9.

2. Rose, J.A., Maizel, J.V., Jr., Inman, J.K., and Shatkin, A.J. (1971). Structural proteins of adenovirus-associated viruses. J. Virol. *8*, 766–770. https://doi.org/10.1128/JVI.8.5.766-770.1971.

3. Elmore, Z.C., Patrick Havlik, L., Oh, D.K., Anderson, L., Daaboul, G., Devlin, G.W., Vincent, H.A., and Asokan, A. (2021). The membrane associated accessory protein is an adeno-associated viral egress factor. Nat. Commun. *12*, 6239. https://doi.org/10.1038/s41467-021-26485-4.

4. Sonntag, F., Schmidt, K., and Kleinschmidt, J.A. (2010). A viral assembly factor promotes AAV2 capsid formation in the nucleolus. Proc. Natl. Acad. Sci. USA *107*, 10220–10225. https://doi.org/10.1073/pnas.1001673107.

5. Zhang, R., Cao, L., Cui, M., Sun, Z., Hu, M., Zhang, R., Stuart, W., Zhao, X., Yang, Z., Li, X., et al. (2019). Adeno-associated virus 2 bound to its cellular receptor AAVR. Nat. Microbiol. *4*, 675–682. https://doi.org/10.1038/s41564-018-0356-7.

6. Zhang, R., Xu, G., Cao, L., Sun, Z., He, Y., Cui, M., Sun, Y., Li, S., Li, H., Qin, L., et al. (2019). Divergent engagements between adeno-associated viruses with their cellular receptor AAVR. Nat. Commun. *10*, 3760. https://doi.org/10.1038/s41467-019-11668-x.

7. Bucher, K., Rodríguez-Bocanegra, E., Dauletbekov, D., and Fischer, M.D. (2021). Immune responses to retinal gene therapy using adeno-associated viral vectors - Implications for treatment success and safety. Prog. Retin. Eye Res. *83*, 100915. https://doi.org/10.1016/j.preteyeres.2020.100915.

8. Sarkar, H., and Moosajee, M. (2022). Choroideremia: molecular mechanisms and therapies. Trends Mol. Med. *28*, 378–387. https://doi.org/10.1016/j.molmed.2022.02.011.

9. Ail, D., Malki, H., Zin, E.A., and Dalkara, D. (2023). Adeno-Associated Virus (AAV) - Based Gene Therapies for Retinal Diseases: Where are We? Appl. Clin. Genet. *16*, 111–130. https://doi.org/10.2147/TACG.S383453.

10. Cideciyan, A.V., Jacobson, S.G., Beltran, W.A., Sumaroka, A., Swider, M., Iwabe, S., Roman, A.J., Olivares, M.B., Schwartz, S.B., Komáromy, A.M., et al. (2013). Human retinal gene therapy for Leber congenital amaurosis shows advancing retinal degeneration despite enduring visual improvement. Proc. Natl. Acad. Sci. USA *110*, E517–E525. https://doi.org/10.1073/pnas.1218933110.

11. Castro, B., Steel, J.C., and Layton, C.J. (2024). AAV-mediated gene therapies for glaucoma and uveitis: are we there yet? Expert Rev. Mol. Med. *26*, e9. https://doi.org/10.1017/erm.2024.4.

12. Koilkonda, R.D., Yu, H., Chou, T.H., Feuer, W.J., Ruggeri, M., Porciatti, V., Tse, D., Hauswirth, W.W., Chiodo, V., Boye, S.L., et al. (2014). Safety and effects of the vector for the Leber hereditary optic neuropathy gene therapy clinical trial. JAMA Ophthalmol. *132*, 409–420. https://doi.org/10.1001/jamaophthalmol.2013.7630.

13. McClements, M.E., Staurenghi, F., Visel, M., Flannery, J.G., MacLaren, R.E., and Cehajic-Kapetanovic, J. (2021). AAV Induced Expression of Human Rod and Cone Opsin in Bipolar Cells of a Mouse Model of Retinal Degeneration. Biomed. Res. Int. *2021*, 1–8. https://doi.org/10.1155/2021/4014797.

14. Ferla, R., Pugni, E., Lupo, M., Tiberi, P., Fioretto, F., Perota, A., Duchi, R., Lagutina, I., Gesualdo, C., Rossi, S., et al. (2025). Retinal gene therapy for Stargardt disease with dual AAV intein vectors is both safe and effective in large animal models. Sci. Adv. *11*, eadt9354. https://doi.org/10.1126/sciadv.adt9354.

15. Maguire, A.M., High, K.A., Auricchio, A., Wright, J.F., Pierce, E.A., Testa, F., Mingozzi, F., Bennicelli, J.L., Ying, G.S., Rossi, S., et al. (2009). Age-dependent effects of RPE65 gene therapy for Leber's congenital amaurosis: a phase 1 dose-escalation trial. Lancet *374*, 1597–1605. https://doi.org/10.1016/S0140-6736(09)61836-5.

16. Wang, J.H., Gessler, D.J., Zhan, W., Gallagher, T.L., and Gao, G. (2024). Adeno-associated virus as a delivery vector for gene therapy of human diseases. Signal Transduct. Target. Ther. *9*, 78. https://doi.org/10.1038/s41392-024-01780-w.

17. Maguire, A.M., Bennett, J., Aleman, E.M., Leroy, B.P., and Aleman, T.S. (2021). Clinical Perspective: Treating RPE65-Associated Retinal Dystrophy. Mol. Ther. *29*, 442–463. https://doi.org/10.1016/j.ymthe.2020.11.029.

18. Dalkara, D., Byrne, L.C., Klimczak, R.R., Visel, M., Yin, L., Merigan, W.H., Flannery, J.G., and Schaffer, D.V. (2013). In vivo-directed evolution of a new adeno-associated virus for therapeutic outer retinal gene delivery from the vitreous. Sci. Transl. Med. *5*, 189ra76. https://doi.org/10.1126/scitranslmed.3005708.

19. Grishanin, R., Vuillemenot, B., Sharma, P., Keravala, A., Greengard, J., Gelfman, C., Blumenkrantz, M., Lawrence, M., Hu, W., Kiss, S., and Gasmi, M. (2019). Preclinical Evaluation of ADVM-022, a Novel Gene Therapy Approach to Treating Wet Age-Related Macular Degeneration. Mol. Ther. *27*, 118–129. https://doi.org/10.1016/j.ymthe.2018.11.003.

20. Kiss, S., Grishanin, R., Nguyen, A., Rosario, R., Greengard, J.S., Nieves, J., Gelfman, C.M., and Gasmi, M. (2020). Analysis of Aflibercept Expression in NHPs following Intravitreal Administration of ADVM-022, a Potential Gene Therapy for nAMD.

Mol. Ther. Methods Clin. Dev. *18*, 345–353. https://doi.org/10.1016/j.omtm.2020.06.007.

21. Khanani, A.M., Thomas, M.J., Aziz, A.A., Weng, C.Y., Danzig, C.J., Yiu, G., Kiss, S., Waheed, N.K., and Kaiser, P.K. (2022). Review of gene therapies for age-related macular degeneration. Eye (Lond) *36*, 303–311. https://doi.org/10.1038/s41433-021-01842-1.

22. Cui, M., Su, Q., Yip, M., McGowan, J., Punzo, C., Gao, G., and Tai, P.W.L. (2024). The AAV2.7m8 capsid packages a higher degree of heterogeneous vector genomes than AAV2. Gene Ther. *31*, 489–498. https://doi.org/10.1038/s41434-024-00477-7.

23. Guo, J., Lin, L.F., Oraskovich, S.V., Rivera de Jesús, J.A., Listgarten, J., and Schaffer, D.V. (2024). Computationally guided AAV engineering for enhanced gene delivery. Trends Biochem. Sci. *49*, 457–469. https://doi.org/10.1016/j.tibs.2024.03.002.

24. Hsu, H.L., Brown, A., Loveland, A.B., Lotun, A., Xu, M., Luo, L., Xu, G., Li, J., Ren, L., Su, Q., et al. (2020). Structural characterization of a novel human adeno-associated virus capsid with neurotropic properties. Nat. Commun. *11*, 3279. https://doi.org/10.1038/s41467-020-17047-1.

25. Tseng, Y.S., and Agbandje-McKenna, M. (2014). Mapping the AAV Capsid Host Antibody Response toward the Development of Second Generation Gene Delivery Vectors. Front. Immunol. *5*, 9. https://doi.org/10.3389/fimmu.2014.00009.

26. Gao, G., Vandenberghe, L.H., Alvira, M.R., Lu, Y., Calcedo, R., Zhou, X., and Wilson, J.M. (2004). Clades of Adeno-associated viruses are widely disseminated in human tissues. J. Virol. *78*, 6381–6388. https://doi.org/10.1128/JVI.78.12.6381-6388.2004.

27. Lakshmanan, R.V., Hull, J.A., Berry, L., Burg, M., Bothner, B., McKenna, R., and Agbandje-McKenna, M. (2022). Structural Dynamics and Activity of B19V VP1u during the pHs of Cell Entry and Endosomal Trafficking. Viruses *14*, 1922. https://doi.org/10.3390/v14091922.

28. Kurian, J.J., Lakshmanan, R., Chmely, W.M., Hull, J.A., Yu, J.C., Bennett, A., McKenna, R., and Agbandje-McKenna, M. (2019). Adeno-Associated Virus VP1u Exhibits Protease Activity. Viruses *11*, 399. https://doi.org/10.3390/v11050399.

29. Lins-Austin, B., Patel, S., Mietzsch, M., Brooke, D., Bennett, A., Venkatakrishnan, B., Van Vliet, K., Smith, A.N., Long, J.R., McKenna, R., et al. (2020). Adeno-Associated Virus (AAV) Capsid Stability and Liposome Remodeling During Endo/Lysosomal pH Trafficking. Viruses *12*, 668. https://doi.org/10.3390/v12060668.

30. Venkatakrishnan, B., Yarbrough, J., Domsic, J., Bennett, A., Bothner, B., Kozyreva, O.G., Samulski, R.J., Muzyczka, N., McKenna, R., and Agbandje-McKenna, M. (2013). Structure and dynamics of adeno-associated virus serotype 1 VP1-unique N-terminal domain and its role in capsid trafficking. J. Virol. *87*, 4974–4984. https://doi.org/10.1128/JVI.02524-12.

31. Dudek, A.M., Zabaleta, N., Zinn, E., Pillay, S., Zengel, J., Porter, C., Franceschini, J.S., Estelien, R., Carette, J.E., Zhou, G.L., and Vandenberghe, L.H. (2020). GPR108 Is a Highly Conserved AAV Entry Factor. Mol. Ther. *28*, 367–381. https://doi.org/10.1016/j.ymthe.2019.11.005.

32. Buning, H. (2020). AAV Entry: Filling in the Blanks. Mol. Ther. *28*, 346–347. https://doi.org/10.1016/j.ymthe.2020.01.015.

33. Loeb, E.J., Havlik, P.L., Elmore, Z.C., Rosales, A., Fergione, S.M., Gonzalez, T.J., Smith, T.J., Benkert, A.R., Fiflis, D.N., and Asokan, A. (2024). Capsid-mediated control of adeno-associated viral transcription determines host range. Cell Rep. *43*, 113902. https://doi.org/10.1016/j.celrep.2024.113902.

34. Qin, W., Xu, G., Tai, P.W.L., Wang, C., Luo, L., Li, C., Hu, X., Xue, J., Lu, Y., Zhou, Q., et al. (2021). Large-scale molecular epidemiological analysis of AAV in a cancer patient population. Oncogene *40*, 3060–3071. https://doi.org/10.1038/s41388-021-01725-5.

35. Zhang, H., Yang, B., Mu, X., Ahmed, S.S., Su, Q., He, R., Wang, H., Mueller, C., Sena-Esteves, M., Brown, R., et al. (2011). Several rAAV vectors efficiently cross the blood-brain barrier and transduce neurons and astrocytes in the neonatal mouse central nervous system. Mol. Ther. *19*, 1440–1448. https://doi.org/10.1038/mt.2011.98.

36. Pillay, S., Meyer, N.L., Puschnik, A.S., Davulcu, O., Diep, J., Ishikawa, Y., Jae, L.T., Wosen, J.E., Nagamine, C.M., Chapman, M.S., and Carette, J.E. (2016). An essential receptor for adeno-associated virus infection. Nature *530*, 108–112. https://doi.org/10.1038/nature16465.

37. Madigan, V.J., Berry, G.E., Tyson, T.O., Nardone-White, D., Ark, J., Elmore, Z.C., Murlidharan, G., Vincent, H.A., and Asokan, A. (2020). The Golgi Calcium ATPase Pump Plays an Essential Role in Adeno-associated Virus Trafficking and Transduction. J. Virol. *94*, e01604. https://doi.org/10.1128/JVI.01604-20.

38. Ding, W., Zhang, L.N., Yeaman, C., and Engelhardt, J.F. (2006). rAAV2 traffics through both the late and the recycling endosomes in a dose-dependent fashion. Mol. Ther. *13*, 671–682. https://doi.org/10.1016/j.ymthe.2005.12.002.

39. Riyad, J.M., and Weber, T. (2021). Intracellular trafficking of adeno-associated virus (AAV) vectors: challenges and future directions. Gene Ther. *28*, 683–696. https://doi.org/10.1038/s41434-021-00243-z.

40. Summerford, C., and Samulski, R.J. (1998). Membrane-associated heparan sulfate proteoglycan is a receptor for adeno-associated virus type 2 virions. J. Virol. *72*, 1438–1445. https://doi.org/10.1128/JVI.72.2.1438-1445.1998.

41. Cheng, S.Y., Luo, Y., Malachi, A., Ko, J., Su, Q., Xie, J., Tian, B., Lin, H., Ke, X., Zheng, Q., et al. (2021). Low-Dose Recombinant Adeno-Associated Virus-Mediated Inhibition of Vascular Endothelial Growth Factor Can Treat Neovascular Pathologies Without Inducing Retinal Vasculitis. Hum. Gene Ther. *32*, 649–666. https://doi.org/10.1089/hum.2021.132.

42. Wang, Q., Li, T., Wu, Z., Wu, Q., Ke, X., Luo, D., and Wang, H. (2013). Novel VEGF decoy receptor fusion protein conbercept targeting multiple VEGF isoforms provide remarkable anti-angiogenesis effect in vivo. PLoS One *8*, e70544. https://doi.org/10.1371/journal.pone.0070544.

43. Xie, H., Ju, H., Lu, J., Wang, X., and Peng, H. (2024). Comparative study on the efficacy of Conbercept and Aflibercept in the treatment of neovascular age-related macular degeneration. Sci. Rep. *14*, 11997. https://doi.org/10.1038/s41598-024-62536-8.

44. Poor, S.H., Qiu, Y., Fassbender, E.S., Shen, S., Woolfenden, A., Delpero, A., Kim, Y., Buchanan, N., Gebuhr, T.C., Hanks, S.M., et al. (2014). Reliability of the mouse model of choroidal neovascularization induced by laser photocoagulation. Invest. Ophthalmol. Vis. Sci. *55*, 6525–6534. https://doi.org/10.1167/iovs.14-15067.

45. Wang, F., Bai, Y., Yu, W., Han, N., Huang, L., Zhao, M., Zhou, A., Zhao, M., and Li, X. (2013). Anti-angiogenic effect of KH902 on retinal neovascularization. Graefes Arch. Clin. Exp. Ophthalmol. *251*, 2131–2139. https://doi.org/10.1007/s00417-013-2392-6.

46. Zhang, M., Yu, D., Yang, C., Xia, Q., Li, W., Liu, B., and Li, H. (2009). The pharmacology study of a new recombinant human VEGF receptor-fc fusion protein on experimental choroidal neovascularization. Pharm. Res. *26*, 204–210. https://doi.org/10.1007/s11095-008-9718-9.

47. Brown, H.C., Doering, C.B., Herzog, R.W., Ling, C., Markusic, D.M., Spencer, H.T., Srivastava, A., and Srivastava, A. (2020). Development of a Clinical Candidate AAV3 Vector for Gene Therapy of Hemophilia B. Hum. Gene Ther. *31*, 1114–1123. https://doi.org/10.1089/hum.2020.099.

48. Ling, C., Lu, Y., Kalsi, J.K., Jayandharan, G.R., Li, B., Ma, W., Cheng, B., Gee, S.W.Y., McGoogan, K.E., Govindasamy, L., et al. (2010). Human hepatocyte growth factor receptor is a cellular coreceptor for adeno-associated virus serotype 3. Hum. Gene Ther. *21*, 1741–1747. https://doi.org/10.1089/hum.2010.075.

49. Excoffon, K.J.D.A., Koerber, J.T., Dickey, D.D., Murtha, M., Keshavjee, S., Kaspar, B.K., Zabner, J., and Schaffer, D.V. (2009). Directed evolution of adeno-associated virus to an infectious respiratory virus. Proc. Natl. Acad. Sci. USA *106*, 3865–3870. https://doi.org/10.1073/pnas.0813365106.

50. Korsnes, M.S., and Korsnes, R. (2018). Single-Cell Tracking of A549 Lung Cancer Cells Exposed to a Marine Toxin Reveals Correlations in Pedigree Tree Profiles. Front. Oncol. *8*, 260. https://doi.org/10.3389/fonc.2018.00260.

51. Holehonnur, R., Luong, J.A., Chaturvedi, D., Ho, A., Lella, S.K., Hosek, M.P., and Ploski, J.E. (2014). Adeno-associated viral serotypes produce differing titers and differentially transduce neurons within the rat basal and lateral amygdala. BMC Neurosci. *15*, 28. https://doi.org/10.1186/1471-2202-15-28.

52. Cabanes-Creus, M., Hallwirth, C.V., Westhaus, A., Ng, B.H., Liao, S.H.Y., Zhu, E., Navarro, R.G., Baltazar, G., Drouyer, M., Scott, S., et al. (2020). Restoring the natural tropism of AAV2 vectors for human liver. Sci. Transl. Med. *12*, eaba3312. https://doi.org/10.1126/scitranslmed.aba3312.

53. Berry, G.E., and Asokan, A. (2016). Cellular transduction mechanisms of adeno-associated viral vectors. Curr. Opin. Virol. *21*, 54–60. https://doi.org/10.1016/j.coviro.2016.08.001.

54. Hull, J.A., Fusco, R.M., Tan, J., Ochoa, M.A., Hall, A., Wan, X., Loeb, E., and Asokan, A. (2025). Functional orthogonality of parvoviral phospholipase A(2) domains in adeno-associated virus transduction. J. Virol. *99*, e0079925. https://doi.org/10.1128/jvi.00799-25.

55. Sauter, M.M., Noel, H.R., Sinha, D., Nelson, E.C., Xiong, M.N., Gamm, D.M., and Brandt, C.R. (2025). AAV2.7m8 transduction of stage 2 human retinal organoids induces highly variable responses in innate and inflammatory gene expression and cytokine secretion. Exp. Eye Res. *258*, 110478. https://doi.org/10.1016/j.exer.2025.110478.

56. Akimoto, M., Cheng, H., Zhu, D., Brzezinski, J.A., Khanna, R., Filippova, E., Oh, E.C.T., Jing, Y., Linares, J.L., Brooks, M., et al. (2006). Targeting of GFP to newborn rods by Nrl promoter and temporal expression profiling of flow-sorted photoreceptors. Proc. Natl. Acad. Sci. USA *103*, 3890–3895. https://doi.org/10.1073/pnas.0508214103.

57. Meisen, W.H., Nejad, Z.B., Hardy, M., Zhao, H., Oliverio, O., Wang, S., Hale, C., Ollmann, M.M., and Collins, P.J. (2020). Pooled Screens Identify GPR108 and TM9SF2 as Host Cell Factors Critical for AAV Transduction. Mol. Ther. Methods Clin. Dev. *17*, 601–611. https://doi.org/10.1016/j.omtm.2020.03.012.

58. Powell, S.K., Samulski, R.J., and McCown, T.J. (2020). AAV Capsid-Promoter Interactions Determine CNS Cell-Selective Gene Expression In Vivo. Mol. Ther. *28*, 1373–1380. https://doi.org/10.1016/j.ymthe.2020.03.007.

59. Stieger, K., Lhériteau, E., Moullier, P., and Rolling, F. (2009). AAV-mediated gene therapy for retinal disorders in large animal models. ILAR J. *50*, 206–224. https://doi.org/10.1093/ilar.50.2.206.

60. Li, H. (2013). Aligning Sequence Reads, Clone Sequences and Assembly Contigs with BWA-MEM. Preprint at (Oxford University Press).

61. Gao, G., and Sena-Esteves, M. (2012). Introducing Genes into Mammalian Cells: Viral Vectors. Mol. Cloning A Lab. Man. *2*, 1209–1313.

62. Afgan, E., Sloggett, C., Goonasekera, N., Makunin, I., Benson, D., Crowe, M., Gladman, S., Kowsar, Y., Pheasant, M., Horst, R., and Lonie, A. (2015). Genomics Virtual Laboratory: A Practical Bioinformatics Workbench for the Cloud. PLoS One *10*, e0140829. https://doi.org/10.1371/journal.pone.0140829.

63. Berry, G.E., and Tse, L.V. (2017). Virus Binding and Internalization Assay for Adeno-associated Virus. Bio. Protoc. *7*, e2110. https://doi.org/10.21769/BioProtoc.2110.

64. Fazzini, F., Schöpf, B., Blatzer, M., Coassin, S., Hicks, A.A., Kronenberg, F., and Fendt, L. (2018). Plasmid-normalized quantification of relative mitochondrial DNA copy number. Sci. Rep. *8*, 15347. https://doi.org/10.1038/s41598-018-33684-5.

YMTHE, Volume *34*

Supplemental Information

Modification of the VP1u region boosts transduction of adeno-associated virus vectors for ocular gene therapy

Mengtian Cui, Shun-Yun Cheng, Jialing Liang, Jackson McGowan, Meiyu Xu, Guangchao Xu, Li Luo, Joae Wu, Christine D. Harman, Amanda L. Jacobson, Lydia E. Kapeller, Melaney A. Mayes, Suk Namkung, Tapan Sharma, Thomas B. Leland, Fang Zhang, Mitchell Yip, Brian Rossmiller, Thomas Xue, Xiupeng Chen, Wassamon Boonying, Anoushka Lotun, Dan Wang, Qin Su, Jun Xie, Yuquan Wei, Ann M. Rothstein, Meredith S. Gregory-Ksander, Andras Komaromy, Bo Tian, Haijiang Lin, Claudio Punzo, Phillip W.L. Tai, and Guangping Gao

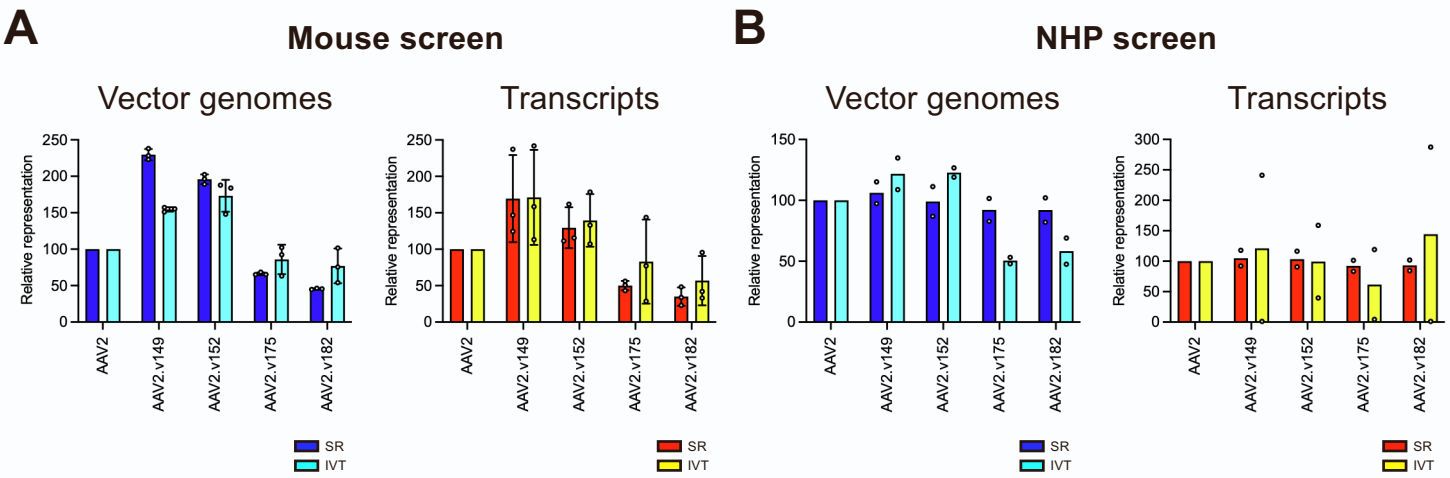

Figure S1. Performance of the top four AAV2 variants in mouse and NHP retinas. Histogram display of data depicted in **Fig. 1B and C**. Values from the library screen in mice **(A)** and NHPs **(B)** are displayed to show detection of vector genomes (left histograms) and transcripts (right histograms) conferred by AAV2, AAV2.v149, AAV2.v152, AAV2.v 175, and AAV2.v182 transduction. Data from subretinal (SR, blue and red) and intravitreal (IVT, cyan and yellow) injections are shown.

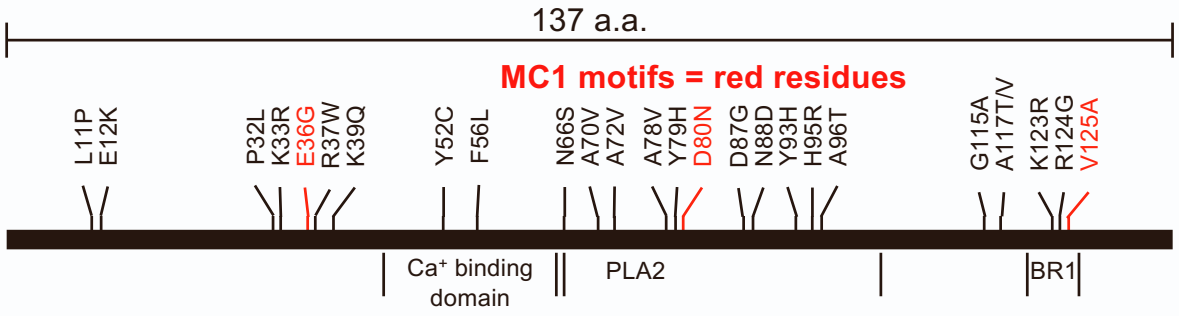

Figure S2. Viral protein (VP) composition of AAV2 variants and the AAV2.MC1 capsid. Diagram of the 137 amino acid AAV2 VP1u sequence showing the distinct residues identified among the AAV2 variants. MC1 residues (red) are highlighted.

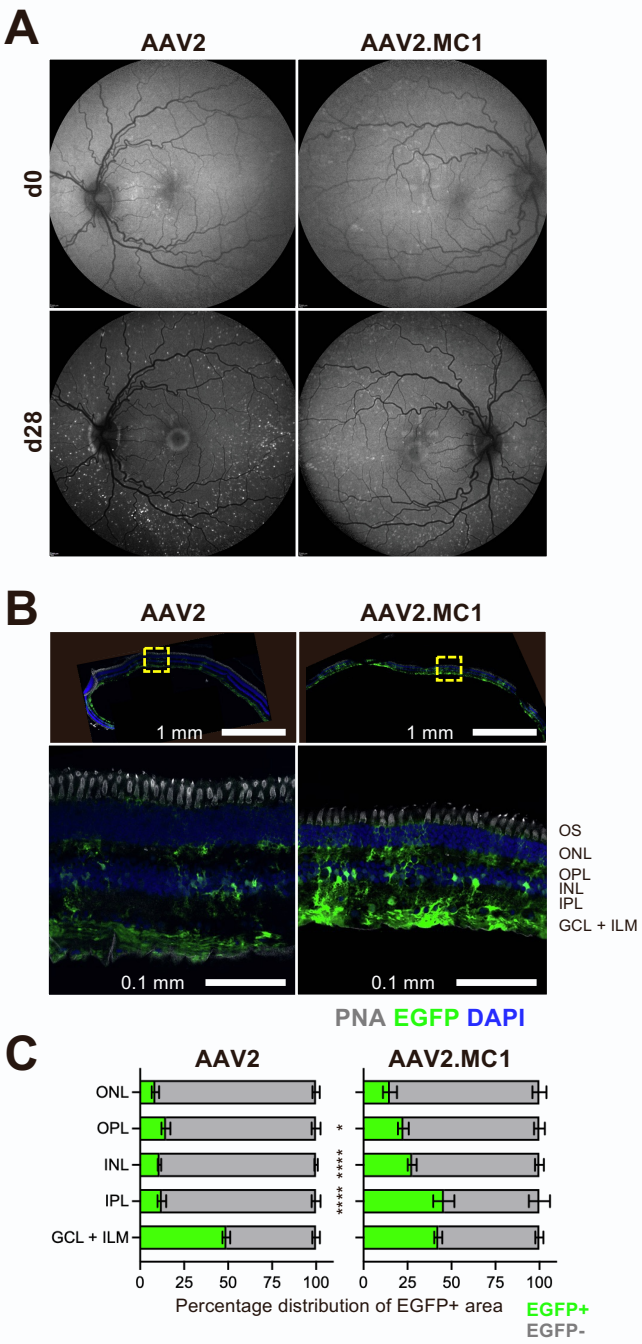

Figure S3. Comparisons of vector transduction in NHP retinas by AAV2.MC1. scAAV-*CB6-Egfp* vectors packaged with AAV2, or AAV2.MC1 were injected into the eyes of one cynomolgus macaque by IVT injection (1E11 vg/eye, 80 μL). **(A)** Fundus autofluorescence images of treated NHPs eyes at days 0 (d0) and 28 (d28) post-injection. **(B)** Cryosections of treated retinas. Sections were stained with peanut agglutinin **(**PNA, cone outer segments), antibodies against EGFP (green), and DAPI (DNA, blue). Bottom row images are zoom-ins of boxed regions from top row images. Scale bars accompany each panel. **(C)** Stacked histograms representing the percentage distribution of EGFP-positive cells across different layers of the retina. *, p <0.05; ****, p <0.0001. Layers of the retina, photoreceptor segment layer (PS), outer nuclear layer (ONL), outer plexiform layer (OPL), inner nuclear layer (INL), inner plexiform layer (IPL), ganglion cell layer (GCL), and inner limiting membrane (ILM) are marked.

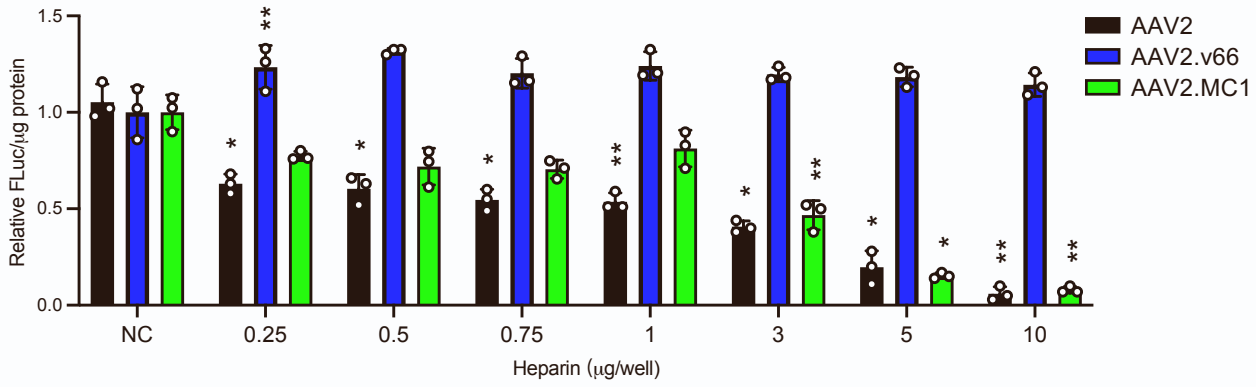

Figure S4. Heparin competition assay comparing the transduction efficiency of AAV2, AAV2.v66, and AAV2.MC1 vectors packaged with firefly luciferase transgenes in HEK293, and in the presence of increasing concentrations of heparin. Luminescence values were scaled to values obtained for wells lacking heparin and set to 1.0. Values represent means ±SD, n=3. *, p <0.05; **, p <0.01 by two-way ANOVA.

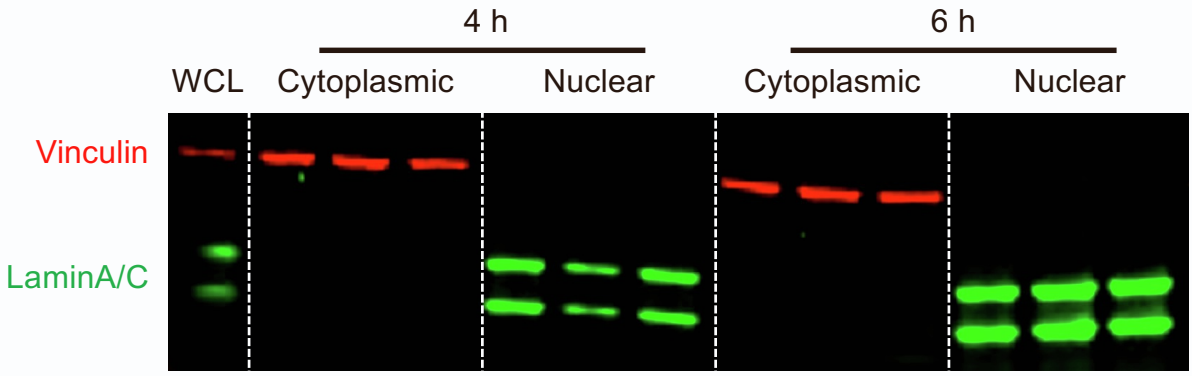

Figure S5. Validation of cytoplasmic and nuclear fraction separation of transduced HeLa cells. To gauge successful separation of cytoplasmic and nuclear fractions, 10 μL of each fraction from individual samples (n=3) were examined by Western blot using antibodies against vinculin (cytoplasmic protein, red) and lamin A/C (nuclear protein, green). Whole cell lysates (WCL) were loaded as a control.

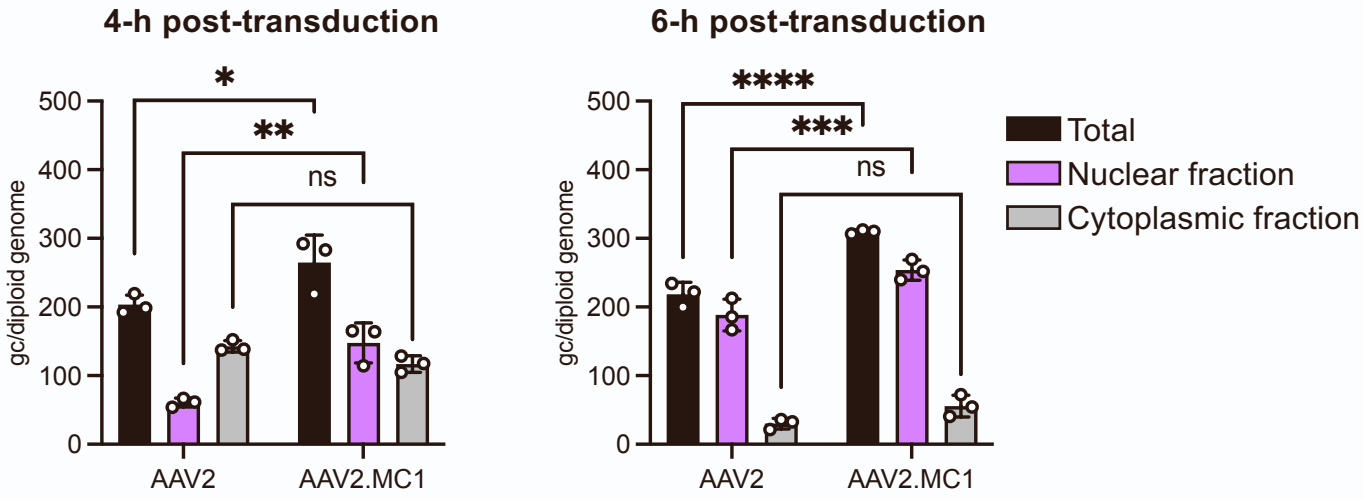

Figure S6. Abundances of genome copies detected in nuclear and cytoplasmic fractions. Genome copies were detected with total cell lysates (black), in cytoplasmic (gray), and in nuclear (purple) fractions of cells treated with AAV2 or AAV2.MC1 vectors at 4- and 6-hours post-transduction. Values were obtained from ddPCR of vector genomes per diploid cell genome (RNase P) in total and nuclear extracted material. Cytoplasmic genomes were calculated by subtracting genome abundances in nuclear extracts from total genomes detected in whole-cell lysates. All values represent means ±SD, n=3. *, p <0.05; **, p <0.01; ***, p <0.001; ****, p <0.0001

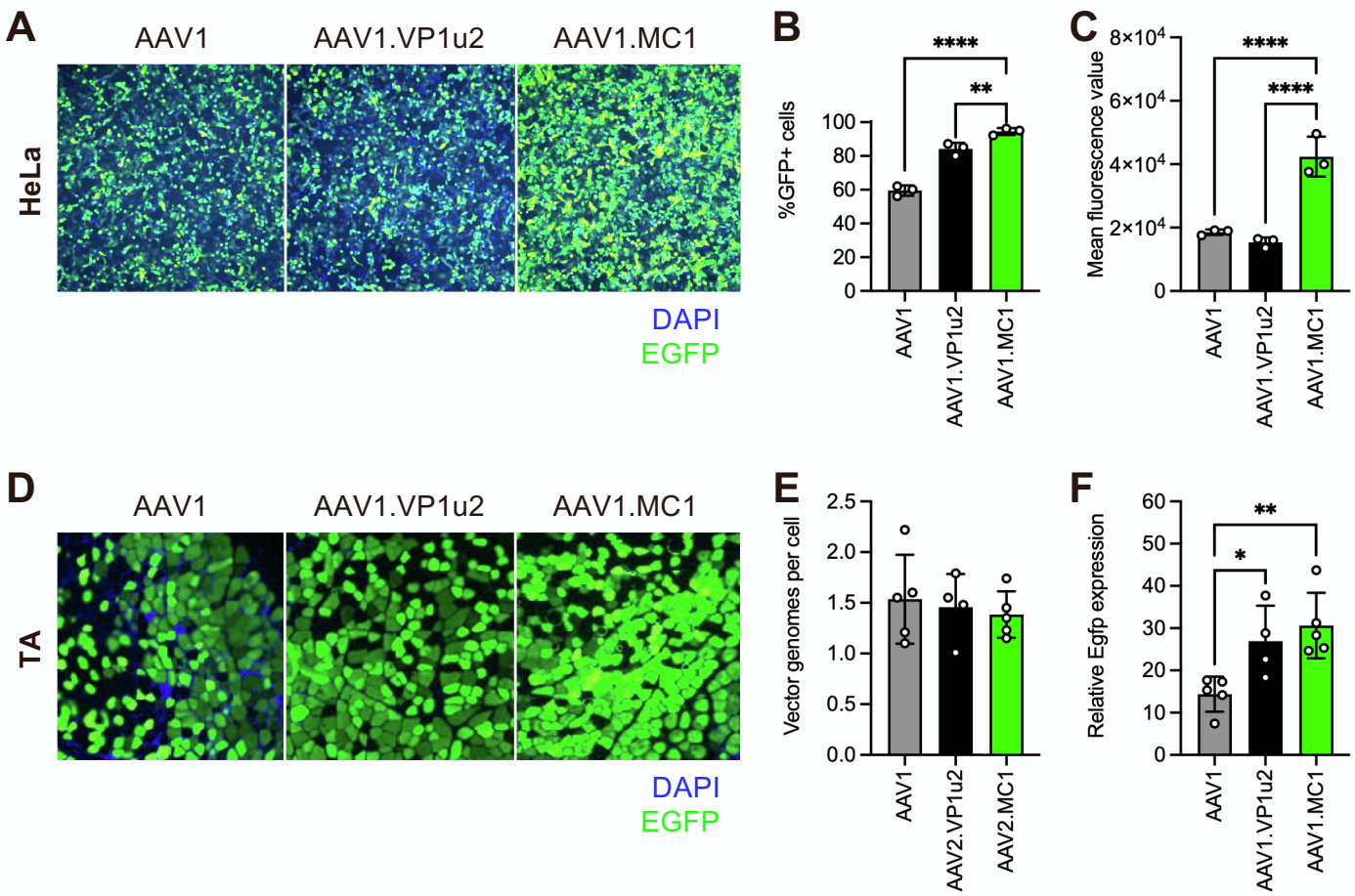

Figure S7. Grafting the MC1 VP1u domain onto AAV1 boosts transduction. (A-C) Assessment of vector transduction by AAV1, and AAV1.VP1u2, and AAV1.MC1 vectors packaged with sc*CB6-Egfp* in HeLa cells 24-h post-transduction (MOI = 1.0E5 vg/cell) as gauged by epifluorescence imaging **(A)** and flow cytometry to measure the percentage of EGFP-positive cells **(B)** and mean fluorescence **(C). (D-F)** Vector transduction was tested in mouse skeletal muscles by intramuscular injection (5.0E10 vg/limb). One-month post-infection, mice were sacrificed, and TA muscles were dissected, stained, and imaged **(D)**. ddPCR analyses was performed on the tissues to quantify the presence of vector genomes **(E)** and *egfp* transcripts **(F)**. For images, EGFP (green) and DAPI (DNA, blue) are shown. For histograms, values represent means ±SD (n≥3). *, p <0.05; **, p <0.01; and ****, p <0.001.

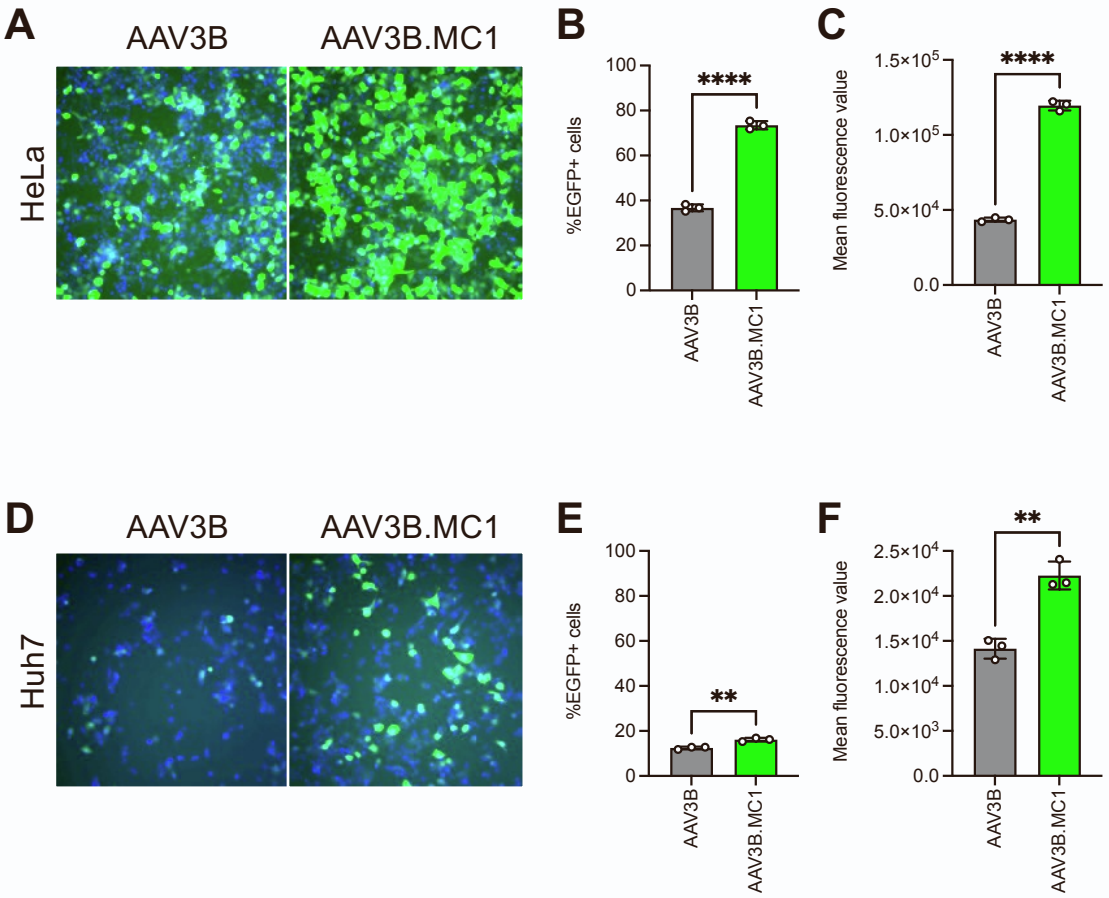

Figure S8. Grafting the MC1 VP1u domain onto AAV3B boosts transduction. (A-C) Assessment of vector transduction by AAV3B and AAV3B.MC1 vectors packaged with sc*CB6-Egfp* in HeLa cells 24-h post-transduction (MOI = 5.0E5 vg/cell) as gauged by epifluorescence imaging **(A)** and flow cytometry to measure the percentage of EGFP-positive cells **(B)** and mean fluorescence **(C). (D-F)** Vector transduction was tested in Huh7 cells (MOI = 5.0E5 vg/cell). Epifluorescence imaging of cells 24-h post-transduction **(D),** flow cytometry to measure the percentage of EGFP-positive cells **(E),** and mean fluorescence **(F)** were performed to gauge transduction**.** For images, EGFP (green) and DAPI (DNA, blue) are shown. For histograms, values represent means ±SD (n≥3). **, p <0.01; ****, p <0.0001. Significance determined by Student's t-test.

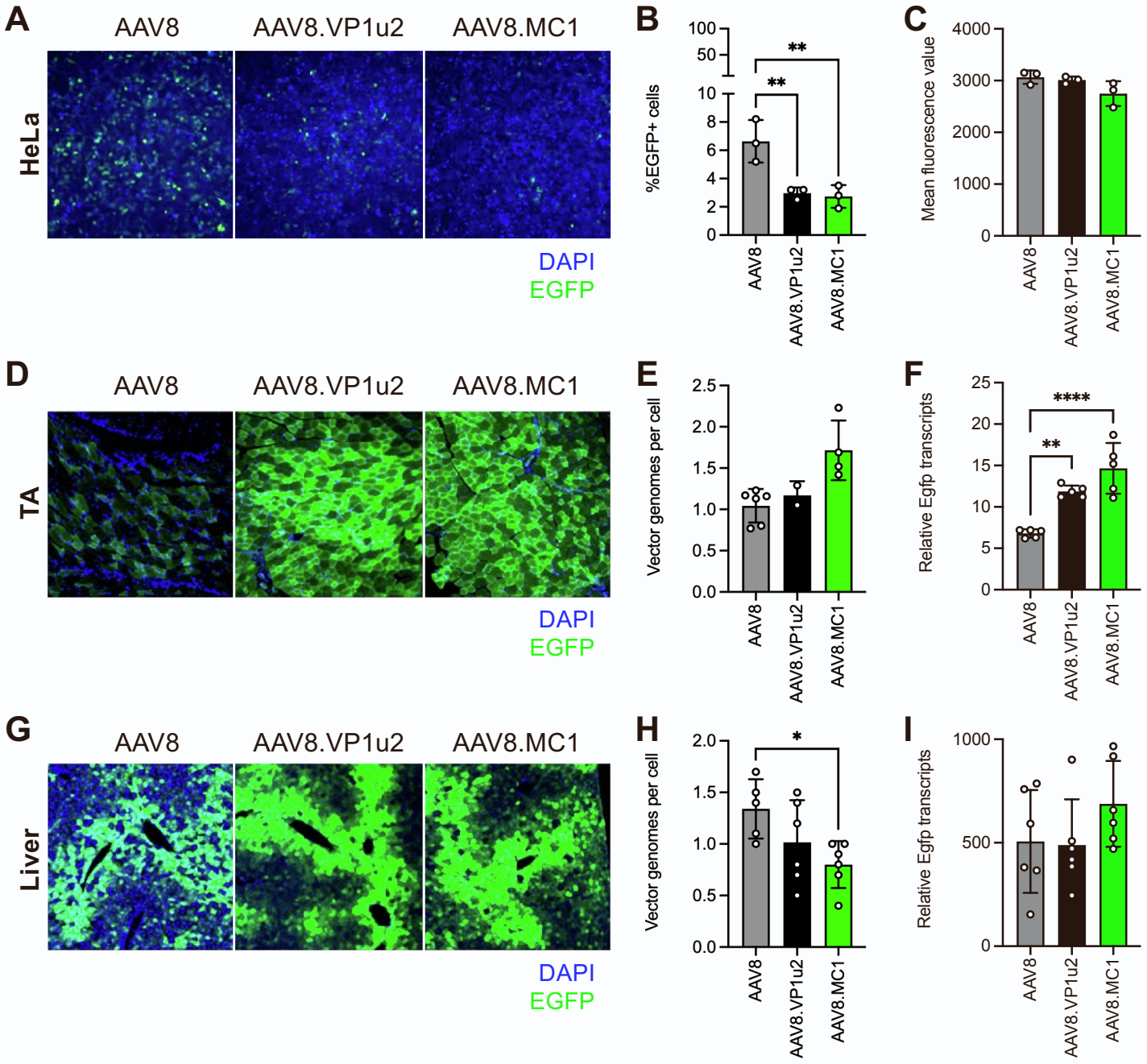

Figure S9. Grafting the MC1 VP1u domain onto AAV8 boosts transduction in a tissue-dependent manner. (A-C) Assessment of vector transduction by AAV8, AAV8.MC1, and AAV8.VP1u2 vectors packaged with sc*CB6-Egfp* in HeLa cells 24 h post-transduction *(*MOI = *5*.0E5 vg/cell) as gauged by epifluorescence imaging **(A)** and flow cytometry to measure the percentage of EGFP+ cells **(B)** and mean fluorescence **(C). (D-I)** Vector transduction was also tested in mouse skeletal muscles and livers following intravenous (tail-vein) injection (1.0E11 vg/mouse). After one-month post-injection, mice were sacrificed and TA muscles and livers were dissected, stained, and imaged **(D and G)**. qPCR analyses were also performed on the tissues to quantify the presence of vector genomes **(E and H)** and *egfp* transcripts **(F and I)**. For images, EGFP (green) and DAPI (DNA, blue) are shown. For histograms, values represent means ±SD (n≥3). *, p <0.05; and ns, not significant.

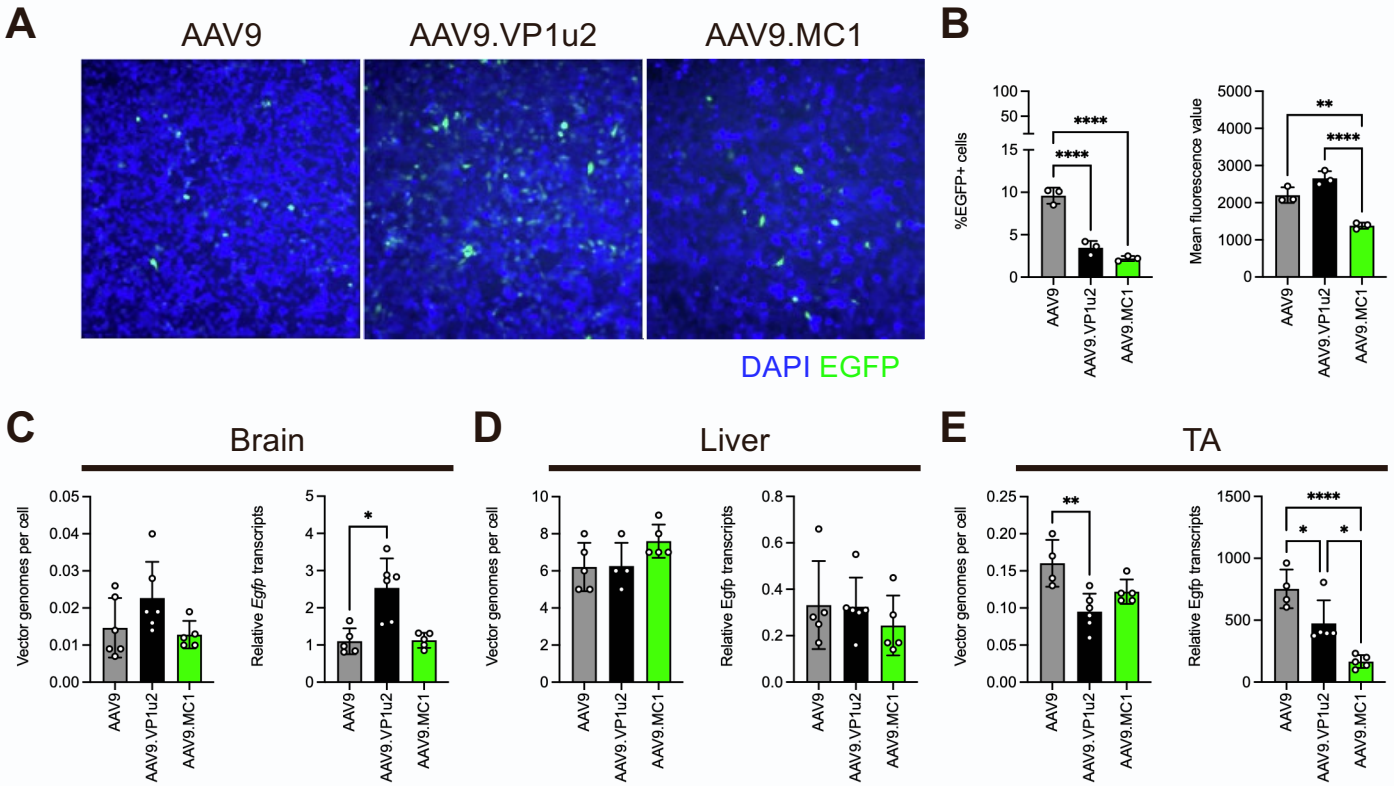

Figure S10. Grafting the MC1 VP1u domain onto AAV9 does not boosts transduction. (A and B) Assessment of vector transduction by AAV9, AAV9.VP1u2, and AAV9.MC1 vectors packaged with sc*CB6-Egfp* in HeLa cells 24-h post-transduction (MOI = 5.0E5 vg/cell) as gauged by epifluorescence imaging **(A)** and flow cytometry **(B)** to measure the percentage of EGFP-positive cells (left) and mean fluorescence (right). EGFP (green) and DAPI (DNA, blue) are shown. **(C-E)** Vector transductions were also tested in neonatal mice following intravenous (facial-vein) injection. One-month post-injection, mice were sacrificed, and brains **(C)**, livers **(D)** and TA muscles **(E)** were dissected and subjected to ddPCR analyses to quantify the presence of vector genomes (left graphs) and *egfp* transcripts (right graphs). For histograms, values represent means ±SD (n≥3). **, p <0.01 and ns, not significant.

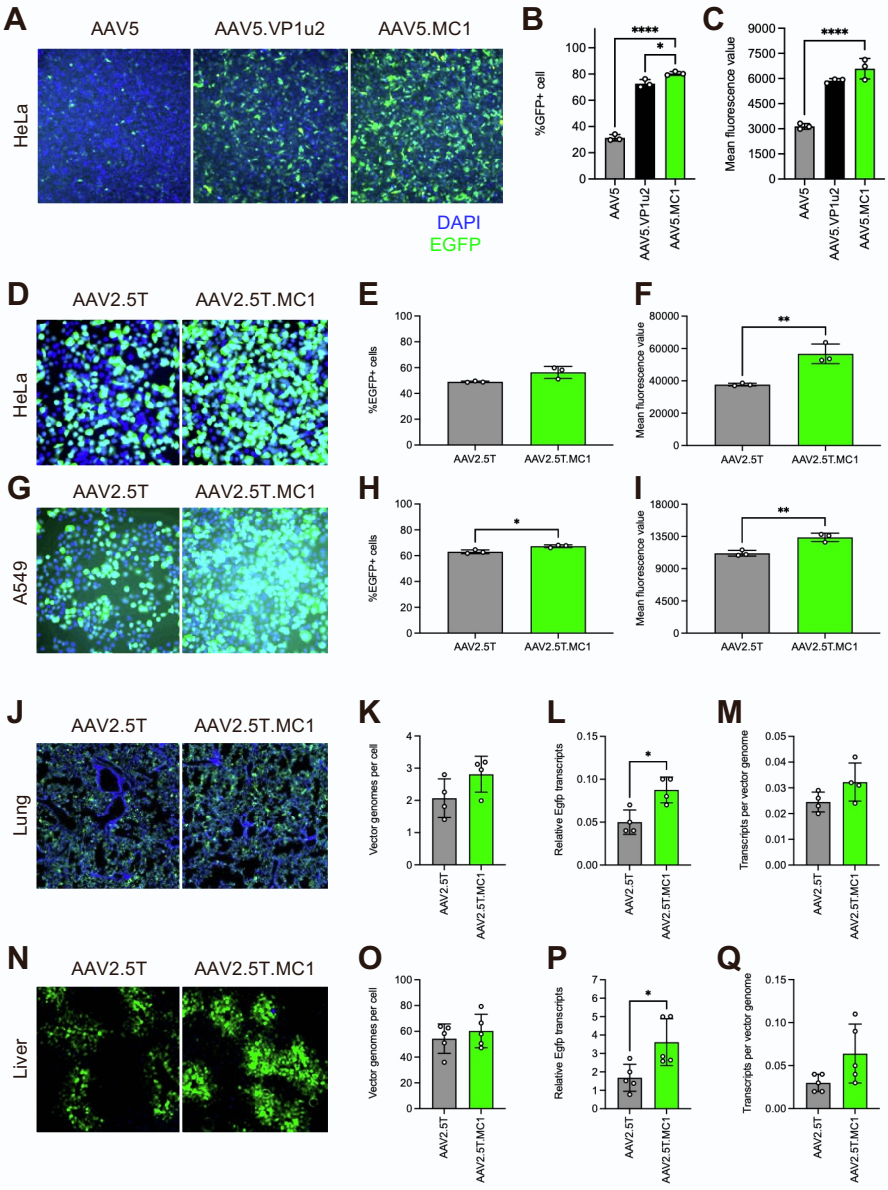

Figure S11. Grafting the MC1 VP1u domain onto AAV5 and AAV2.5T boosts transduction. **(A-C)** Assessment of vector transduction by AAV5, AAV5.VP1u2, and AAV5.MC1 vectors packaged with *CB6.PI.Egfp* in HeLa cells 24-h post-transduction (MOI = 1.0E5 vg/cell) as gauged by epifluorescence imaging **(A)** and flow cytometry to measure the percentage of EGFP-positive cells **(B)** and mean fluorescence **(C).** **(D-I)** Assessment of vector transduction by AAV2.5T, and AAV2.5T.MC1 vectors packaged with *CB6.PI.Egfp* in HeLa and A549 cells 24-h post-transduction (MOI = 4.0E5 vg/cell) as gauged by epifluorescence imaging **(D and G)** and flow cytometry to measure the percentage of EGFP-positive cells **(E and H)** and mean fluorescence **(F and I).** **(J-Q)** Vector transduction was tested in mouse livers and lungs following intravenous delivery (1.0E11 vg/mouse). Three-weeks post-injection, mice were sacrificed, and liver and lung tissues were dissected, stained, and imaged **(J and N)**. ddPCR analyses were also performed on the tissues to quantify the presence of vector genomes **(K and O)** and *egfp* transcripts **(L and P)**. Transcripts per vector genome were also calculated **(M and Q)**. For images, EGFP (green) and DAPI (DNA, blue) are shown. For histograms, values represent means ±SD (n≥3). *, p <0.05; **, p <0.01; and ****, p <0.0001.

Table S1. Summary of primer sets used for generating VP1 capsid mutations

Capsid	Forward primer (5'-3')	Reverse primer (5'-3')
AAV2 *trans* plasmid backbone (HindIII & BsiwI)	ACGTCAGACGCGGAAGCTTCGATCAACTACGC	AGTACCAGCTCCCGTACGTCCTCGGCTC
AAV2.E36G	CACCAAAGCCCGCAGGGCGGCATAAGGAC	GTCCTTATGCCGCCCTGCGGGCTTTGGTG
AAV2.D80N	ACAAAGCCTACAACCGGCAACTCGACAGCG	GCTGTCGAGTTGCCGGTTGTAGGCTTTGTC
AAV2.V125A	GCGAAAAAGAGGGCTCTTGAACCTCTG	CAGAGGTTCAAGAGCCCTCTTTTTCGCCTG
AAV2.5T *trans* plasmid backbone (HindIII & PflMI)	ACGTCAGACGCGGAAGCTTCGATCAACTACGC	CCGGGGCAAAGTCCACAAACTGGGGGTCGTTG

Table S2. Summary of PCR amplicon primers used to detect genome and transcript barcodes in tissues treated with AAV2 variant libraries

Primer name	Sequence (5'-3')
bcEGFP-amp-For-1	AGAGTACTGTAAAGCGGCCATCAAGCTCAAC
bcEGFP-amp-For-2	CGTGTGCAGTAAAGCGGCCATCAAGCTCAAC
bcEGFP-amp-For-3	ATGTATCTGTAAAGCGGCCATCAAGCTCAAC
bcEGFP-amp-For-4	GACTCGACGTAAAGCGGCCATCAAGCTCAAC
bcEGFP-amp-For-5	CGATGACGGTAAAGCGGCCATCAAGCTCAAC
bcEGFP-amp-For-6	CACACGTAGTAAAGCGGCCATCAAGCTCAAC
bcEGFP-amp-For-7	GCTGTATCGTAAAGCGGCCATCAAGCTCAAC
bcEGFP-amp-rev	CATTTTATTAGGAAAGGACAGTGGGAGTGG
bcEGFP-RT	GACACCTACTCAGACAATG

Table S3. Summary of ddPCR probe sets and and catalogue IDs.

Target gene	Probe	Assay ID
gDNA and transcription	Egfp-FAM	Mr00660654_cn
Mouse DNA loading control	Tfrc-VIC	4458366
Mouse cDNA loading control	Gapdh-VIC for lung	Mm99999915_g1
	Gusb-VIC for retina	Mm01197698_m1
Human cell lines cDNA loading control	Hprt1-VIC	Hs03929098_m1
Human cell lines DNA loading control	RNase P-VIC	4403326

TableS4.xlsx. Excel file of barcode raw reads attributed to each of the packaged capsid variants for mouse and NHP retinas injected with libraries via subretinal or intravitreal delivery. Data divided into separate sheets. Counts of barcodes from the preinjection vector library was used to normalize counts. Values were scaled to AAV2 abundances set to 100 and are the final values reported in **Figs. 1 and S1**.